RESEARCH ARTICLE

Key Points:
- Six years record of temperature, current, turbidity, and bioluminescence in the convection zone of the northwestern Mediterranean
- Strong currents associated to bottom-reaching convection induce deep sediment resuspension and formation of aggregates in the water column
- Upward transfer of resuspended sediment, stimulated by eddy activity, produces thick, and long-lasting bottom nepheloid layers

Correspondence to:
X. Durrieu de Madron,
demadron@univ-perp.fr

Deep sediment resuspension and thick nepheloid layer generation by open-ocean convection

X. Durrieu de Madron[1] iD, S. Ramondenc[2] iD, L. Berline[3] iD, L. Houpert[4] iD, A. Bosse[5] iD, S. Martini[6], L. Guidi[2] iD, P. Conan[7] iD, C. Curtil[8], N. Delsaut[1], S. Kunesch[1] iD, J. F. Ghiglione[7], P. Marsaleix[8] iD, M. Pujo-Pay[7], T. Séverin[9,10] iD, P. Testor[5] iD, C. Tamburini[3], and the ANTARES collaboration[11]

[1]Université de Perpignan Via Domitia, CNRS, CEFREM, Perpignan, France, [2]Sorbonne Universités, UPMC Université Paris 06, CNRS, Laboratoire d'Océanographie de Villefranche (LOV), Observatoire Océanologique, Villefranche-sur-mer, France, [3]CNRS-IRD, Université d'Aix-Marseille, UMR 7294–IRD 235, MIO, Marseille, France, [4]SAMS, Scottish Marine Institute, Oban, Argyll, UK, [5]Sorbonne Universités, UPMC Université Paris 06, CNRS-IRD-MNHN, UMR 7159, Laboratoire d'Océanographie et de Climatologie, IPSL, Paris, France, [6]Monterey Bay Aquarium Research Institute (MBARI), Moss landing, California, USA, [7]Sorbonne Universités, UPMC Université Paris 06, UMR 7621, Laboratoire d'Océanographie Microbienne, Observatoire Océanologique, Banyuls sur mer, France, [8]CPPM, CNRS, Marseille, France, [9]Université de Toulouse, CNRS, UPS, Laboratoire d'Aérologie Toulouse, France, [10]Marine Science Institute, The University of Texas at Austin, Port Aransas, Texas, USA, [11]See Appendix A

Abstract The Gulf of Lions in the northwestern Mediterranean is one of the few sites around the world ocean exhibiting deep open-ocean convection. Based on 6 year long (2009–2015) time series from a mooring in the convection region, shipborne measurements from repeated cruises, from 2012 to 2015, and glider measurements, we report evidence of bottom thick nepheloid layer formation, which is coincident with deep sediment resuspension induced by bottom-reaching convection events. This bottom nepheloid layer, which presents a maximum thickness of more than 2000 m in the center of the convection region, probably results from the action of cyclonic eddies that are formed during the convection period and can persist within their core while they travel through the basin. The residence time of this bottom nepheloid layer appears to be less than a year. In situ measurements of suspended particle size further indicate that the bottom nepheloid layer is primarily composed of aggregates between 100 and 1000 μm in diameter, probably constituted of fine silts. Bottom-reaching open ocean convection, as well as deep dense shelf water cascading that occurred concurrently some years, lead to recurring deep sediments resuspension episodes. They are key mechanisms that control the concentration and characteristics of the suspended particulate matter in the basin, and in turn affect the bathypelagic biological activity.

1. Introduction

1.1. Attributes of Bottom Nepheloid Layers in the World Ocean

In the open ocean, the distribution of particulate matter in the water column presents distinct turbid layers. The photic layer at the surface is primarily associated to planktonic organisms and is highly time variable in its thickness and intensity. Underneath this surface nepheloid layer (SNL), particulate matter concentration presents a decreasing gradient, and a broad minimum at varying intermediate depths. *Biscaye and Eittreim* [1977] showed from vertical profiles of light scattering in the Atlantic that concentrations at clear water minimum are one-to-two orders of magnitude lower than those in surface water but still reflect the residual flux of surface-water biological production and surface circulation patterns, suggesting that the "background" turbidity level in the oceans is primarily a function of the biogenic fallout.

Below the clear water minimum, a rise of the particle concentration toward the bottom has been observed from nephelometric observations in various regions of the ocean, i.e., the Atlantic [*Biscaye and Eittreim*, 1977; *Eittreim et al.*, 1975, 1976; *Ewing et al.*, 1971; *McCave*, 1986, *Nyffeler and Godet*, 1986; *Vangriesheim and Khripounoff*, 1990], in the Gulf of Mexico [*Feely*, 1975], at the foot of the continental slope off Washington [*Baker*, 1976], off northern New Zealand [*McCave and Carter*, 1997], over the ridges and rises surrounding the Canada basin in the arctic [*Hunkins et al.*, 1969], and more recently in the northwestern Mediterranean [*Béthoux et al.*, 2002; *Puig et al.*, 2013]. These bottom nepheloid layers (BNL) are referred to the suspended particles concentration below clear water, which is in excess of the clear water minimum concentration.
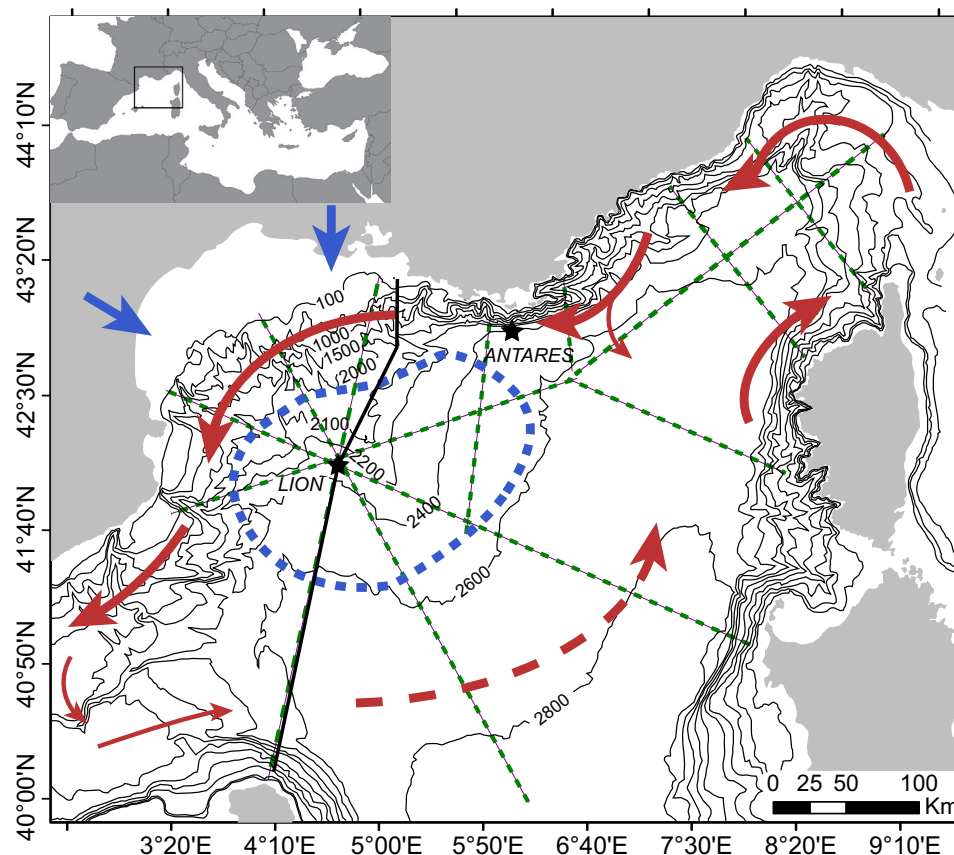
Figure 1. Map of the northwestern Mediterranean. Red arrows underline the cyclonic general circulation. Blue arrows indicate the predominant NW (Tramontane) and N (Mistral) winds, and the blue dashed line delineates the main convection region. The black stars show the position of the LION mooring line in the center of open-ocean convection region (blue dashed line), and the ANTARES mooring line at the base of the continental slope. The black solid line indicates the MOOSE T02 glider endurance line. The green dashed lines indicated the CTD sections carried out during the different cruises (see Table 1).

They present thicknesses varying from few hundreds of meters to 1–2 km, which is far thicker than the frictional boundary layer.

Several studies emphasized that deep sediments in oceanic basins may be actively resuspended and redistributed to form deep BNL. The most intense BNL are found in areas of strong western boundary currents [*Biscaye and Eittreim*, 1977; *McCave and Carter*, 1997] and in regions where the bottom current regime is highly variable due to eddy activity [*McCave*, 1986; *Auffret et al.*, 1994] and internal tide oscillations [*Vangriesheim and Khripounoff*, 1990]. Benthic storms of high kinetic energy and near-bed flow were also observed to resuspend deep bottom sediments and generate large concentrations of suspended sediment [*Gardner and Sullivan*, 1981; *Gross et al.*, 1988; *Gardner et al.*, 2017].

Deep BNLs are then believed to be due to currents that are large enough to entrain and maintain in suspension fine sedimentary material, but their lifetime is still quite uncertain due to the difficulty to monitor them. *Gardner et al.* [1985] suggested that the mean residence time for particles resuspended in the nepheloid layer are on the order of weeks to months, and *Puig et al.* [2013] suggested that thick BNL observed in the northwestern Mediterranean could even last several years. The dynamics of BNL is closely related to the particle size and settling velocity. While the latter parameter has seldom been estimated for particles from the BNL, several studies [*McCave*, 1983, 1984; *McCave and Gross*, 1991, *Puig et al.*, 2013] inferred that the particles in the BNL were probably composed of aggregates formed from very fine sedimentary particles.

1.2. Situation in the Gulf of Lions

The Gulf of Lions in the northwestern Mediterranean (Figure 1) is one of the few places around the world where open-ocean deep convection is taking place. This is due to a peculiar setting of the general

circulation with a cyclonic gyre trapping water in the middle of the basin, and significant winter heat losses due to strong northern winds [*Marshall and Schott*, 1999]. Open-ocean convection shows a strong interannual variability of its intensity, particularly in terms of mixed layer depth, that might affect the thermohaline properties of deep waters in the Gulf of Lions [*Mertens and Schott*, 1998; *Béthoux et al.*, 2002; *Font et al.*, 2007; *Puig et al.*, 2013; *Houpert et al.*, 2016]. Dense waters are also formed in the nearby shelf and occasionally cascade down the slope toward the deep basin, interacting with the open sea convection [*Béthoux et al.*, 2002; *Durrieu de Madron et al.*, 2013].

Dense shelf water cascading impact on sediment dynamics and suspended particle transport on the slope and basin has been monitored since 1993 [*Heussner et al.*, 2006; *Canals et al.*, 2006; *Ogston et al.*, 2008; *Puig et al.*, 2008; *Palanques et al.*, 2012]. These studies revealed that massive events of dense shelf water cascading, which occurred in 1999, 2005, and 2006, eroded sediment along the slope and transported large amount of suspended particles in the bottom layer. The exceptional 2005 cascading episode likely supplied large amount of fine sediment from the slope to the basin, as increase of particle fluxes by two orders of magnitude for more than 1 month were observed after the event [*Palanques et al.*, 2009]. In a recent review, *Puig et al.* [2013] showed that thick BNL associated to newly formed deep waters appeared in the basin following these major cascading events, but that the 2005/2006 events apart, the BNL rapidly vanished (i.e., BNL faded away approximately after 1 year). However, subsequently to the 2005/2006 events, the BNL was still present in 2011 after a deep convection occurring in 2009 and 2010 [*Tamburini et al.*, 2013; *Puig et al.*, 2013], while no major cascading event took place during that period and no major (i.e., bottom-reaching) open-ocean convection event occurred in 2007 and 2008.

Major cascading event are invariably associated to major open-ocean convection, which lead to a strong mixing down to the seabed and large near-bottom currents in the ensuing horizontal spreading phase of the newly formed deep water. It is noteworthy that major convection events can nevertheless take place while cascading is weak. Resuspension of deep sediments in the Gulf of Lions solely by the major convection event of 2009 was first evidenced by *Stabholz et al.* [2013]. Hence, it was hypothesized that open-ocean convection could also contribute to the preservation, or even the formation of the BNL. Regardless of the respective role of cascading and convection in the formation of the BNL, the transport mechanisms responsible for its large thickness and extent has not been clarified, and the nature of the suspended particles need to be detailed.

Some preliminary measurements based on *in situ* camera images [*Puig et al.*, 2013] suggested that large aggregates (with a mode around 150 μm) are present throughout the BNL. In addition, deep convection and resuspension also transfer biogeochemical components to the deep waters like oxygen, inorganic, and organic matter, contributing to the ventilation and the "fueling" of the deep pelagic and benthic ecosystems [*Severin et al.*, 2014; *Tamburini et al.*, 2013; *Martini et al.*, 2014].

In the framework of the MOOSE project (Mediterranean Ocean Observing System on Environment; http://www.moose-network.fr/), high frequency and pluriannual observations of hydrology and currents in the convection region were collected without interruption since 2010 from a mooring line. This monitoring is complemented by an annual summer hydrological survey of the northwestern Mediterranean that includes the convection region (MOOSE-GE cruises) [*Testor and Coppola*, 2010]. Besides, in the framework of the MISTRALS-MERMEX project (Marine Ecosystems' response in the Mediterranean Experiment; MERMEX group, 2011), a dedicated experiment was conducted in 2012–2013 to assess the role of deep waters formation in the northwestern Mediterranean on the concentration of key biogenic elements and plankton in the water column over an annual cycle. In this particular context, two hydrological cruises were carried out in winter 2013 [*Testor*, 2013] and spring 2013 [*Conan*, 2013] based on the same network of stations and hence complementary to the MOOSE-GE annual cruises.

On the basis of these new observations, this paper aims at (i) confirming the occurrence of sediment resuspension in the Gulf of Lions during bottom-reaching deep convection events, (ii) evidencing the mechanisms responsible of the upward motion of resuspended particulate matter in the water column, and (iii) describing the characteristics of the BNL (thickness, extent) and the suspended particles (concentrations, size).

2. Material and Methods

The observations were collected using two different types of sampling platforms. Section 2.1 presents spatial measurements (mostly hydrological and optical data) made from ships and glider, whereas section 2.2

Table 1. Dates, Names, Data Sampled, Number of Casts and DOI Reference for the Different Cruises

Dates	Cruise Name	Parameters	CTD Casts	UVP/LISST Casts	DOI
24 Jul–8 Aug 2012	MOOSE-GE 2012	CTD, UVP	87	87/–	10.17600/12020030
3–21 Feb 2013	DEWEX 1	CTD, UVP	75	53/–	10.17600/13020010
5–24 Apr 2013	DEWEX 2	CTD, UVP, LISST	100	73/62	10.17600/13020030
11 Jun–9 Jul 2013	MOOSE-GE 2013	CTD, UVP	41	38/–	10.17600/13450110
4–22 Jul 2014	MOOSE-GE 2014	CTD, UVP	94	68/–	10.17600/14002300
10–27 Jul 2015	MOOSE-GE 2015	CTD, UVP	82	52/–	10.17600/15002500

presents temporal measurements (currents, particulate fluxes, bioluminescence) made from moorings. The different cruises are listed in Table 1. The Ocean Data View software (Schlitzer, R., Ocean Data View, http://odv.awi.de, 2015) was used for the analysis and plotting of the cruise results.

2.1. Observations From Ship and Gliders
2.1.1. Ship-Based Measurements

Conductivity, temperature, depth (CTD) and optical data were acquired during cruises conducted on the R/Vs *Le Suroît* and *Tethys II* in the northwestern Mediterranean. Four MOOSE-GE cruises carried out in the summers of 2012, 2013, 2014, and 2015 (Table 1) are considered here. Two additional cruises were carried out in February 2013 (DEWEX 1) during the strong convection period and in April 2013 (DEWEX 2) during the spring bloom (Table 1). The sampling plan was drawn as star shape sections crossing the cyclonic circulation of the basin (Figure 1).

Standard CTD measurements were obtained from the surface to a few meters above the seafloor with a Sea-Bird Electronics 11plus pumped CTD interfaced with a rosette with twelve 10-litre Niskin bottles. Thirteen data channels were measured at 24 Hz: pressure, two pairs of temperature (SBE3) and conductivity (SBE4), dissolved oxygen (SBE43), light transmission (WetLabs C-Star at 650 nm), chlorophyll fluorescence (Chelsea Aquatracka III), photo synthetically active radiation (QSP-2300), Colored Dissolved Organic Matter (WetLabs ECO-CDOM fluorometer), and altimetry (Tritech PA500). A laser *in situ* scattering and transmission sensor (Sequoia LISST-Deep), and an Underwater Vision Profiler (Hydroptic UVP-5) [*Picheral et al.*, 2010] were also installed on the rosette frame.

LISST and UVP measurements: The LISST-Deep measured the light attenuation and scattering from a red light-emitting diode of 670 nm wavelength at a frequency of 1 Hz. It enables to derive particle volume concentration (in μL L^{-1}) from 1.5 to 250 μm for 32 classes in log10-based increments [*Agrawal and Pottsmith*, 2000]. The LISST-Deep was placed vertically to the side of the CTD frame and the UVP during the DEWEX 2 spring cruise. Valid LISST-Deep profiles were obtained for 13 deep stations (depth > 2000 m) only out of 62 stations; the other profiles showed spurious jumps of the signal at depth that could not be corrected. A background scattering measurement is necessary to compute particle volume from the measured signal. Here, as in *White et al.* [2015], we used the in-situ minimum raw scattering signal at depth, across all valid profiles.

The UVP-5 acquires focus images in a virtual volume of water delimited by a light sheet issued from red light-emitting diodes (LEDs) of 625 nm wavelength at a frequency up to 6 Hz. The smaller size limit is fixed by optical resolution, whereas the larger size limit is determined by the volume of water illuminated per image. Recorded images are automatically digitized, classified, and analyzed, and the results are expressed as concentration of large particles (particles L^{-1}) in 27 log-based size classes between 52 μm and 27 mm.

Optical windows of both instruments were rinsed with MilliQ water and wiped carefully prior to each cast. Measurements were retrieved from the downward casts only.

In order to compare and merge the particle size distribution derived from the LISST-Deep and UVP-5, the UVP-5 measurements were converted in volume concentrations (μL L^{-1}) assuming an equivalent spherical diameter for the median size of each class. Volume measured in the overlapping size classes for the LISST-Deep and UVP-5 (52–66, 83–105, 132–166, and 166–209 μm) showed reasonable agreement for bins 52–66 and 83–105, underestimation of UVP with respect to LISST-Deep for 132–166 and overestimation of UVP with respect to LISST-Deep for 166–209. The combined particle size distribution was finally computed for
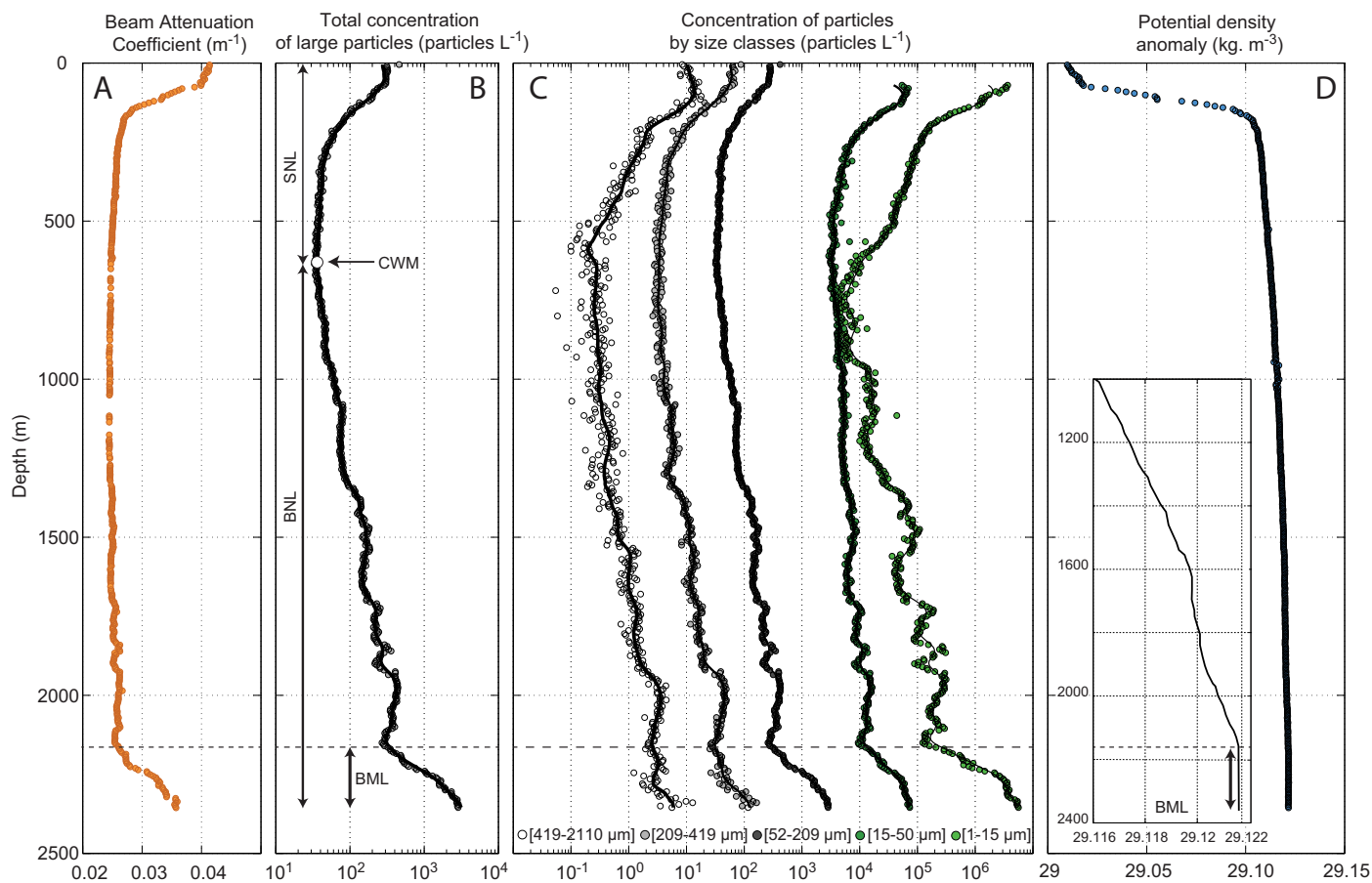
Figure 2. Examples from station 8 of the DEWEX 2 cruise of profiles of (a) beam attenuation coefficient from transmissometer, (b) total large particle concentration from the UVP, (c) size-dependent particle concentration from the LISST-Deep ([1–15 μm], [15–50 μm]) and UVP ([52–209 μm], [209–419 μm], [419–2110 μm]), and (d) potential density anomaly. Clear water minimum (CWM), defined on the profile of total concentration of large particle, sets the limit between the surface nepheloid layer (SNL) and the bottom nepheloid layer (BNL). The upper limit of bottom mixed layer (BML), evidenced on the water density profile, is delineated by a dashed line.

the 13 deep stations having both valid LISST-Deep and UVP data, using LISST-Deep data for size classes from 1.5 to 131 μm and UVP-5 data for size classes from 131 μm up to 27 mm.

The clear water minimum was estimated as the minimum of suspended particle concentration that is usually found below the surface layer and to midwater depth. It corresponded to the minimum total volume concentration for the LISST data, and to the minimum abundance of large particles (>52 μm) for the UVP (Figure 2). The clear water minimum was equally determined for the different particle populations identified from the combined size spectra of the LISST and UVP (Figure 2). BNL is referred to the suspended particles below the clear water minimum, which is in excess of the clear water minimum concentration, and its thickness is calculated as the distance between the clear water minimum and the seabed. The thickness of the bottom mixed layer (BML) is calculated as the near-bottom layer with quasi-homogenous potential density anomaly ($\Delta\sigma_\theta < 0.0005$ kg m^{-3} over the BML).

2.1.2. Glider-Based Measurements
A Teledyne Webb Research Slocum glider sampled the deep basin along an endurance line (MOOSE T02) between Marseille in the north and the Menorca Island in the south (Figure 1). It has a sawtooth trajectory between the surface and 1000 m depth, and achieved a distance around ∼2–6 km between consecutive surfacing. The onboard sensors were an un-pumped SeaBird 41cp CTD, and a Wetlabs FLNTU that provided turbidity (Bb expressed in nephelometric turbidity units—NTU) based on backscattering measurements at 700 nm. *Bourrin et al.* [2015] inferred a calibration relationship for this sensor for coastal waters of the Gulf of Lions ($C_{mg/L} = 1.747 * Bb_{NTU}$).

From its dead reckoning navigation and GPS fixes at surface, the glider also allows to compute a mean current corresponding to the average of horizontal currents over each dive (hereafter referred to as the depth-average currents, DAC). A calibration of the compass of the gliders has been performed before each deployment and this ensures a relative accuracy of about 1 cm s^{-1} for both components of the average currents over deep dives of a few hours. The relative vorticity of the barotropic flow has been estimated from the glider DAC. DACs were first decomposed into their cross-track and along-track components, and then smoothed using a Gaussian moving average according to the along-track distance carried out by the glider. The smoothing scale (Gaussian variance of 2 km) was chosen in order to take into account for the 5–10 km radius eddies that form during deep convection events in the northwestern Mediterranean Sea [*Bosse et al.*, 2016]. Note that gliders, which move at 20–40 km/day relative to the water, are perfectly suited to sample such small-scale vortices [*Bosse et al.*, 2015, 2016]. The vorticity is finally approximated by the along track derivative of the cross-track DAC. This single component might capture most of the signal while crossing oceanic currents at right angle. Hereafter, we describe a sediment resuspension event during which the angle between the glider track and the flow was measured to be 90 ± 10°. So, our glider-based vorticity can be considered as satisfactory in terms of sign, variability and order of magnitude.

2.2. Mooring Observations
2.2.1. Acoustical Current Meter Data
The LION mooring site (Figure 1) is located in the center of the convection zone at 42°02.4′N–4°41.0′E with a water depth of 2350 m. Since 2009, the turnaround of the mooring line occurred once a year in summertime. The line has 25 instruments distributed through depth comprising 10 temperature sensors, 10 CTD sensors, and 5 current meters spanning depths from 150 to 2320 m (see *Houpert et al.* [2016] for a detailed description of the mooring design). Nortek Aquadopp acoustic current meters provided measurements of the horizontal and vertical velocity components of the current, pressure, temperature, and acoustic echo intensity at the nominal depths of 150, 250, 500, 1000, and 2320 m (30 m above the seabed). The current meter's setup with burst sampling (1 Hz sampling during 220 s interval every 30 min) provided horizontal and vertical velocities precision of 0.5 and 0.7 cm s^{-1} respectively. Vertical velocity measurements were corrected from the vertical movements of the line derived from the pressure records.

Suspended particulate matter concentration was estimated from gravimetric measurements. Water samples were filtered up to filter saturation, on pre-weighed Nuclepore filters of 0.4 mm pore size; their solid residue weights yielded suspended sediment concentration (SSC). Triplicates were made for each water sample, and divergent values with respect to the median value were discarded.

Acoustic echo intensity records were converted into suspended particle concentration using an empirical linear equation between the logarithm of concentration (C) and echo intensity (EI) [*Gartner*, 2004]. Given that the echo intensity was often less than 10 dB above noise level, the corrected formulation of *Gostiaux and Van Haren* [2010] that take into account the noise level was used. The equation found using simple regression between concomitant backscatter data and direct sampling concentration in the Gulf of Lions was 10 x log($C_{mg/L}$) = 0.407 * EI_{dB} — 22.55 (r^2 = 0.94, N = 66). The current meter acoustic frequency at 2 MHz leads to a peak sensitivity for particles around 250 μm [*Nortek*, 2001].

2.2.2. Sediment Trap Data
A short mooring line (∼50 m long) was deployed at 42°01′N–4°48′E (depth of 2300 m), about 10 km from the LION mooring. It was equipped with a Technicap PPS-3 sediment trap (collecting area of 0.125 m^2, aspect ratio of 2.5, and 12 collecting cups) at 30 m above the seabed. In 2012–2013, the trap samples were collected during two consecutive periods from 11 August 2012 to 10 November 2012 with sampling interval of 8 days, and from 19 November 2012 to 15 June 2013 with sampling interval between 15 and 24 days. Mass fluxes are normalized by the period of the sample and surface area of the trap. The results are expressed in mg m^{-2} d^{-1}. Prior to deployment, the sampling bottles were filled with 0.45 μm filtered seawater containing sodium borate buffered formalin to yield a final concentration of 5% formalin to prevent *in situ* microbial decomposition. Upon recovery, samples were stored in the dark at 4°C according to the method described by *Heussner et al.* [1990]. Samples were separated in the laboratory into aliquots using a high precision peristaltic pump to obtain equal subsamples of 10–20 mg (dry weight) through repeating splitting of the cleaned raw samples. After removal of swimmers under a dissecting microscope, subsamples for particulate organic carbon (POC) analysis were filtered onto pre-combusted GF/F filters. POC was measured using a VarioMAX CN Elementar analyzer after removing carbonate by acidification with 2 N HCl.

Subsamples for grain size analysis were made using a Malvern 3000 grain sizer after deflocculation by sonification for 5 min.

2.2.3. Bottom Sediment Data

Sediments cores were collected during one cruise next to the LION mooring site using an OKTOPUS GmbH multiple corer allowing the sampling of undisturbed surface sediment. Three surface sediment (0–0.5 cm) samples from three cores were sampled to take into account the local heterogeneity of the seabed. The samples were merged, homogenized, and placed in polyethylene plastic bags, and stored in the dark at −20°C, freeze-dried and homogenized prior to analysis. POC concentration and grain size were measured as for the sediment trap samples.

2.2.4. Bioluminescence Data

Bioluminescence data have been recorded with the ANTARES neutrino telescope from September 2009 to September 2015. The ANTARES neutrino telescope is a cabled observatory located 40 km south of Toulon (42°48′N, 6°10′E) at 2475 m depth in the northwestern Mediterranean Sea [*Ageron et al.*, 2011]. It comprises a three-dimensional array of 885 Hamamatsu R7081-20 photomultiplier tubes (PMTs) distributed on 12 mooring lines. These PMTs are sensitive to the wavelength range of 400–700 nm, which matches the main bioluminescence emission spectrum (440–540 nm) [*Tamburini et al.*, 2013; *Martini et al.*, 2014]. PMT counting rates used for bioluminescence monitoring measure the total number of single photons detected every 105 ms and give the arithmetic mean rates as a mathematical estimator. Therefore, a local polynomial fit has been performed on a 30 min interval in order to be consistent with the oceanographic data sampling rate in this study. The bioluminescence rates were expressed in thousands of photons per second (or kHz). The main light contributions recorded by PMTs partly result from Cherenkov radiation induced by the beta decay of ^{40}K in seawater and from bioluminescence [*Costantini and the ANTARES Collaboration*, 2010]. The Cherenkov radiation induced by the beta decay of ^{40}K in seawater produces a background of about (40 kHz), and is observed to be constant over a period of a few years. All intensity increases over this background (40 kHz) is accepted to be due to bioluminescence [*Tamburini et al.*, 2013].

Two sets of three optical modules belonging to different lines of the telescope have been sequentially used to supply the time series. On a long time scale, the records of light intensity from those OMs are representative of those collected by the whole array of ANTARES PMTs.

3. Results

The results are split in two subsections addressing different time scales. The first subsection addresses the intraannual variability during the 2012–2013 period of the hydrology, currents, suspended particulate matter, and bioluminescence based on the LION and ANTARES mooring time series, respectively, and seasonal cruises. This subsection further contains complementary information on the particle size in the water column, sediment trap, and sediment. It also focuses on a peculiar high turbidity event. The second subsection presents the interannual variability of the hydrology, currents, suspended particulate matter, and bioluminescence based on the mooring time series, and the MOOSE-GE summer cruises.

A comprehensive description of the mixed layer depth variations and convection phases based on all the CTD sensors located on the mooring line and an adjacent surface buoy are presented in *Houpert et al.* [2016]. Fortunately, the main characteristics of convective events are well captured by current meter parameters, which do not present any data gaps and respond to the needs of this work.

3.1. Intraannual Variability During the 2012–2013 Period
3.1.1. Time Series at the Mooring Sites From July 2012 to June 2013

Records of potential temperature, horizontal and vertical current velocity, particulate matter concentrations, total mass and particulate organic carbon fluxes at the LION site, and bioluminescence at the ANTARES site from July 2012 to July 2013 are presented in Figure 3.

The different phases of the open-ocean convection are clearly visible from temperature and current intensity (Figures 3a–3c): (i) an autumn period with a stratified water column with low currents, (ii) a mixing of the surface layer from early December 2012 to mid-January 2013 with enhanced subsurface currents, (iii) a strong mixing period from mid-January 2013 to mid-March 2013 with a cooling and homogenization of the water column and strong vertical velocities, and (iv) a restratification period of the upper water column from mid-March 2013 to late June 2013 with strong barotropic horizontal velocities (from 150 m to the
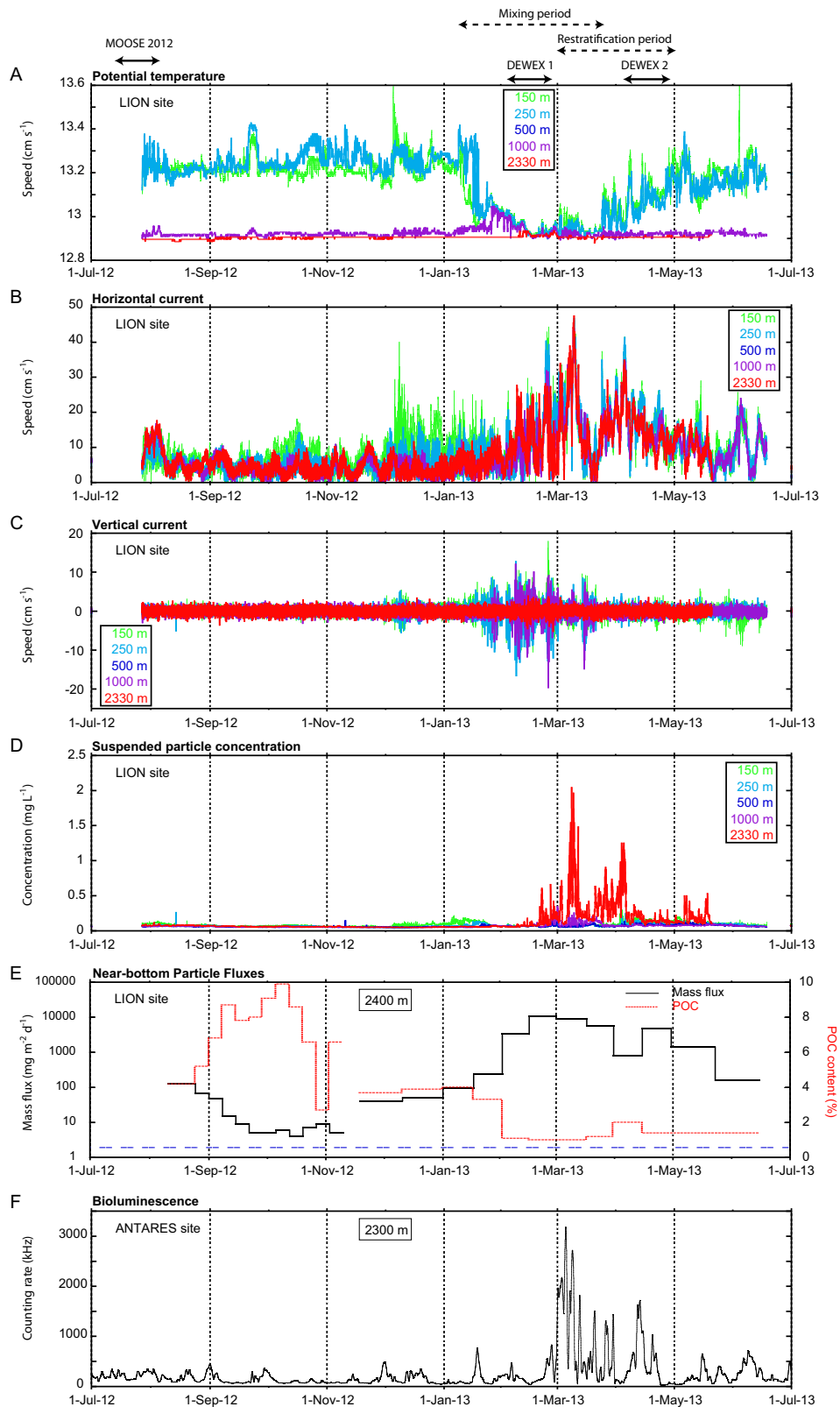
Figure 3. July 2012 to July 2013 time series at the LION site of (a) potential temperature, (b) horizontal current velocities, (c) vertical current velocities, and (d) suspended particulate matter concentration at 150, 250, 500, 1000, and 2330 m nominal depths. (e) Near-bottom total mass flux (black solid line) and particulate organic carbon (POC, red line). The dashed blue line indicated the POC content in surficial sediment at the LION site (0.56%) [*Stabholz et al.*, 2013]. (f) Time series of bioluminescence at the ANTARES site. The period of the cruises (MOOSE-GE 2012 in July 2012, DEWEX1 in February 2013, and DEWEX 2 in April 2013), and of mixing and spreading phases are indicated on the top of the figure.
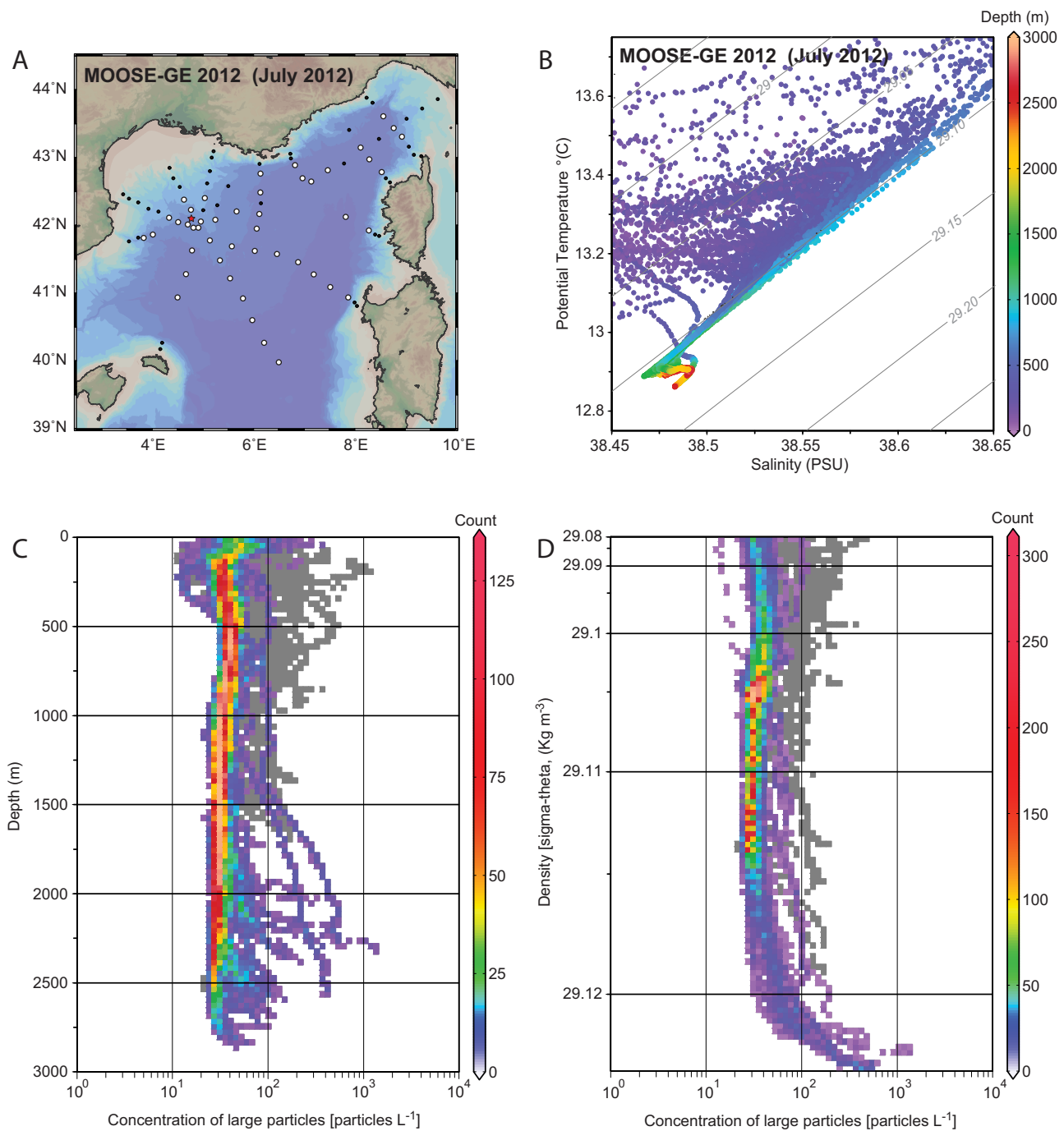
Figure 4. (a) Location of surface to bottom stations during the MOOSE-GE 2012 cruise in July 2012. White circle indicated stations within anomalous suspended particulate matter concentration profiles characterized by significantly increasing concentrations with depth (i.e., BNL). The red star indicates the LION mooring site in the convection region. (b) θ-S diagram in the BNL area in July 2012. (c and d) Statistics of large particles distribution from the UVP measurement in the BNL versus depth and density, respectively. The grey color on the background represents the statistics for all the stations of the MOOSE-GE 2012 cruise.

bottom) but low vertical velocities. Restratification occurs when the surface net heat flux becomes positive, the horizontal currents increase strongly (as seen in Figures 3 and 4) bringing surrounding warmer and stratified waters into the convection zone, while at the same time the newly formed dense waters spread out of the convection area.

Estimates of particulate concentrations at all levels (Figure 3d) are very low and stable (< 0.2 mg L^{-1}) except in early December 2012 when subsurface concentrations slightly increase, probably due to the

deepening of the surface mixed layer richer in planktonic organisms. Concentrations stay low during the early stage of the strong mixing period. They abruptly increase, especially near the bottom, starting in mid-February (when the convection reaches the seabed) and peaks at about 2 mg L^{-1} by mid-March 2013. Afterward, near-bottom concentration remains high, but variable, until mid-May 2013. Small increases of suspended particle concentration are also noticeable at 1000 m in late February and early March 2013. The increase of subsurface concentrations in April and early May 2013 probably relate to the spring planktonic bloom that ensues from the convection period.

Near-bottom particle flux and organic carbon content (Figure 3e) show opposite temporal patterns. Particle flux is rather low (range: 4–243 mg m^{-2} d^{-1}; average: 43 mg m^{-2} d^{-1}) and POC content is high (range: 2.7–9.9%; average: 6.2%) until late January. Starting in late January until late March, particle flux markedly increases (range: 3270–10,339 mg m^{-2} d^{-1}; average: 7079 mg m^{-2} d^{-1}) and organic carbon content shows minimum values (range: 1.0–1.2%; average: 1.1%) close to that of the superficial sediment (0.56%). The increase of flux clearly coincides with the peak of particle concentration and the period of enhanced horizontal currents. Despite the 6-fold reduction of the POC content during winter (from 6.2% to 1.1% on average), the massive increase of particles flux yields a 40-fold increase POC flux (from 1.9 to 74 mg m^{-2} d^{-1} on average). Afterward, particle flux gradually decreases to reach value of about 150 mg m^{-2} d^{-1}, but always with low organic carbon (1.4%). The POC flux decreases to 2 mg m^{-2} d^{-1}.

Bioluminescence measured at the ANTARES site (Figure 3e) shows a temporal variability very similar to that of the horizontal current speed and near-bottom suspended matter concentration at the LION site with a significant increase in March-April 2013 and peaks up to about 3000 kHz (i.e., two orders of magnitude above the background value).

3.1.2. Suspended Particles Distribution During the 2012–2013 Cruises
The results of the summer 2012 cruise (MOOSE-GE 2012, July–August 2012) are depicted in Figure 4. All stations present a strong stratification (Figure 4b) typical of the summer period. The statistical depth distribution of the particles abundance counted by the UVP (Figures 4c and 4d) shows a minimum abundance between 1000 and 2000 m deep (∼30 particles L^{-1}) and for numerous stations an increasing number of particles with depth all the way to the bottom (up to 1000 particles L^{-1}). The resulting bottom nepheloid layers are between few tens of meters up to 2300 m thick. Profiles of abundance versus density reveal that the BNLs are overall aligned with the isopycnals.

During the winter cruise (DEWEX 1, February 2013) only stations in the central part of the convection area (Figure 5a) show nearly homogeneous thermohaline characteristics (Figure 5b). In this area, the particle abundances observed by the UVP also show homogeneous profiles all over the water column with low values (∼10 particles L^{-1}, Figures 5c and 5d). Some stations show, however, a slight increase particle abundances (up to ∼20 particles L^{-1}) in the deep layer. Whereas the other stations out of the convection region are more stratified, the profiles of particle abundance are also very homogeneous below 200 m deep and have similar low values (generally <20 particles L^{-1}).

The spring cruise (DEWEX 2, April 2013) results are depicted in Figure 6. All stations present a restratified water column (Figure 6b). Similarly to July 2012, the particle abundances (Figures 6c and 6d) show a minimum between 500 and 1000 m deep (∼20–30 particles L^{-1}), an increasing number of particles with depth all the way to the bottom (with a maximum abundance of 6200 particles L^{-1}), and an isopycnic distribution.

The thickness of the BNL (i.e., distance between the CWM and the seabed) has been estimated for the deep stations (with bottom depth > 2000 m) during the DEWEX 2 cruise (Figure 7). The mapping reveals that the BNL has the shape of a lens centered on the convection region. Its thickness is about 1800 m next to the LION site and rapidly decreases to the east and south to less than 250 m.

It is noteworthy that for all deep stations presenting a BNL, the bottommost part of the profile shows a marked increase of the turbidity and particle abundance (see Figure 2 as an example). The thickness of this near-bottom intensification matches the thickness of the bottom mixed layer (BML) visible on the water density profile (Figure 2d). The BML is between 15 and 380 m thick (average: 110 m), and is composed of new deep waters formed during the winter.

3.1.3. Characteristics of Particulate Matter
The size distribution of particles for the deep stations (bottom depth >2000 m) derived from the UVP and LISST measurements in the BNL and in the SNL (i.e., respectively, below and above the clear water
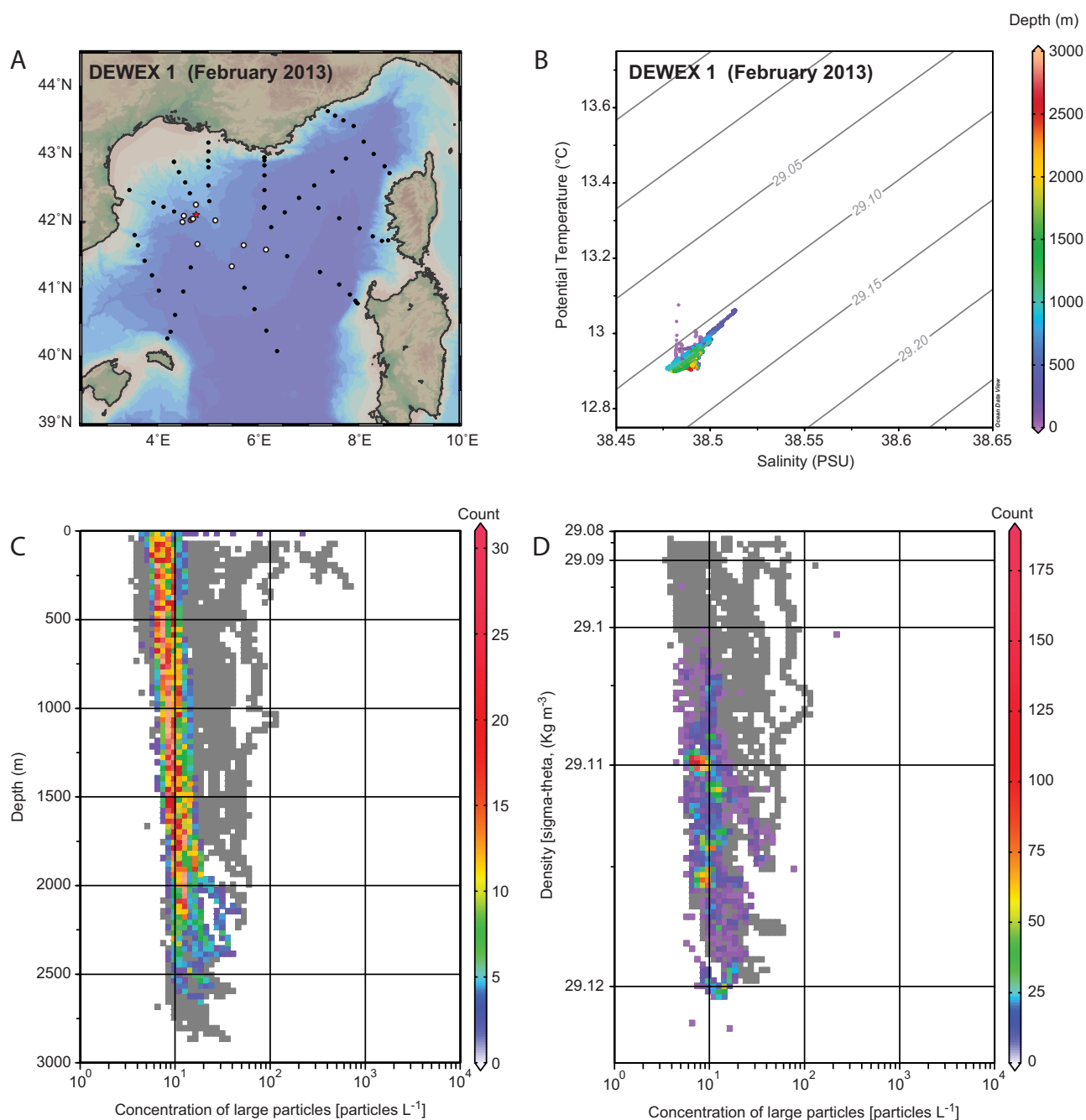
Figure 5. (a) Location of surface to bottom stations during the DEWEX 1 cruise in February 2013. White circle indicated stations within the deep convection region having nearly homogeneous θ-S characteristics throughout the water column. The red star indicates the LION mooring site in the convection region. (b) θ-S diagram of the stations within the convection region, i.e., showing nearly homogeneous θ-S characteristics throughout the water column. (c and d) Statistics of large particles distribution from the UVP measurement versus depth and density, respectively. The grey color on the background represents the statistics for all the stations of the DEWEX 1 cruise.

minimum) during spring are presented in Figure 8. Several modes appear in the BNL (Figure 8a). Two minor modes are seen around 10 and 30 μm, two major modes are seen around 150 and 250 μm, and a significant abundance of coarse particles appear between 500 and 1000 μm. UVP pictures reveal that the large particles in the BNL consists almost solely of aggregates. Particles' size distribution in the SNL (Figure 8b) also evidences similar modes, however, with a larger abundance of particle between 500 and 3000 μm. These coarse particles in the SNL correspond primarily to organic detritus [see *Donoso et al.*, 2017]. Accordingly, the median size of the suspended particles in the SNL ranges between 300 and 600 μm, while it ranges between 100 and 230 μm in the BNL.
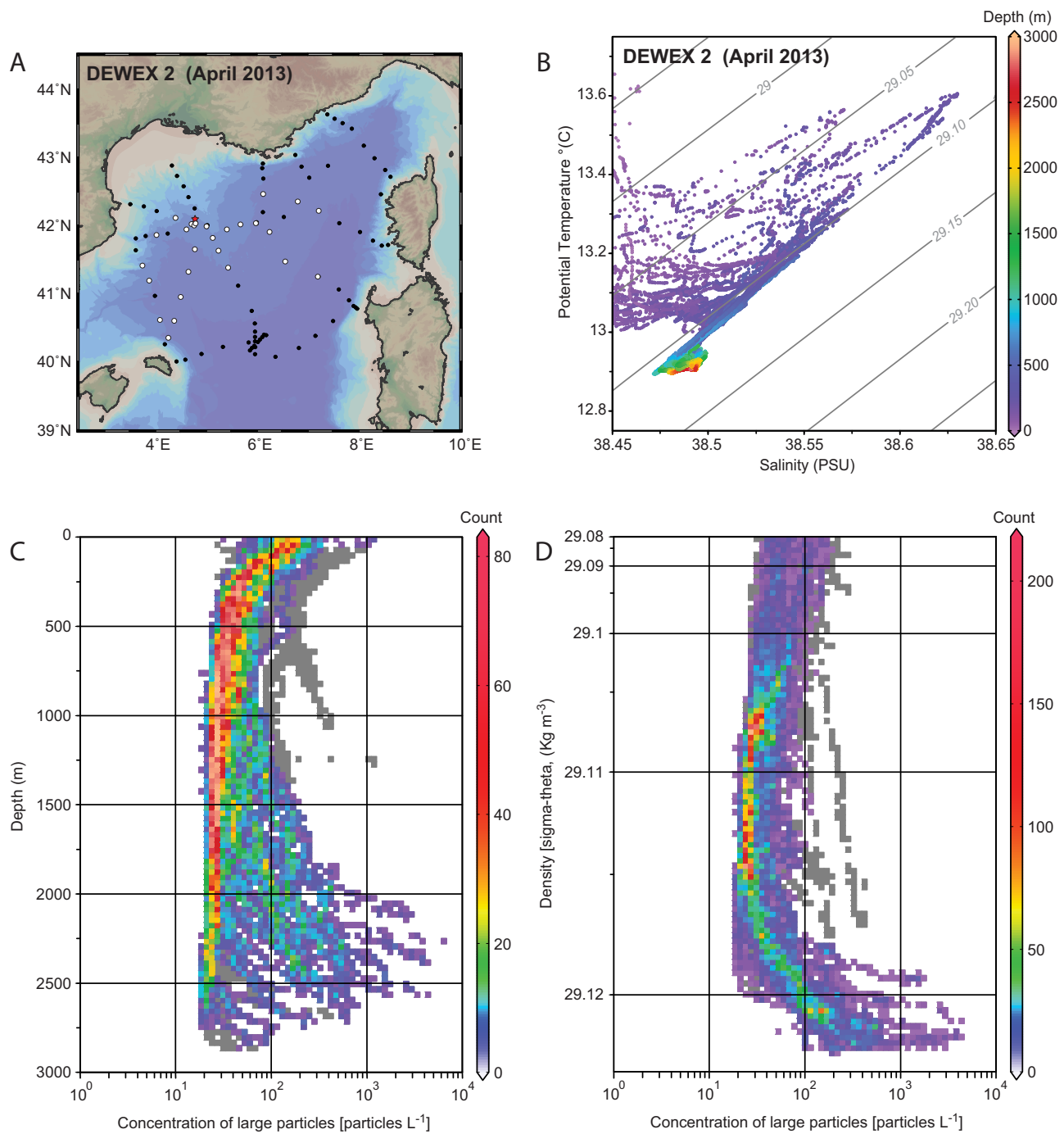
Figure 6. (a) Location of surface to bottom stations during the DEWEX 2 cruise in April 2013. Stations marked by a white circle indicate deep stations (bottom depth > 2000 m) having anomalous profiles of suspended particulate matter concentrations characterized by significantly increasing concentrations with depth (i.e., BNL). The red star indicates the LION mooring site in the convection region. (b) θ-S diagram of the stations showing anomalous suspended particulate matter concentration profiles. (c and d) Statistics of large particles distribution from the UVP measurement versus depth and density, respectively. The grey color on the background represents the statistics for all the stations of the DEWEX 2 cruise.

Deflocculated particle size spectra from near-bottom sediment trap samples collected from early February to late March during the high flux period (Figure 9a), and from local sediment (Figure 9b) show similar distributions dominated by the presence of small primary particles (with a principal mode around 8 μm and a secondary mode around 30 μm), typical of fine and medium silts. In the sediment, the few coarse particles about 2 mm are plankton shell remains (pteropodes are commonly observed in surface sediments) [e.g., *Zúñiga et al.*, 2007].
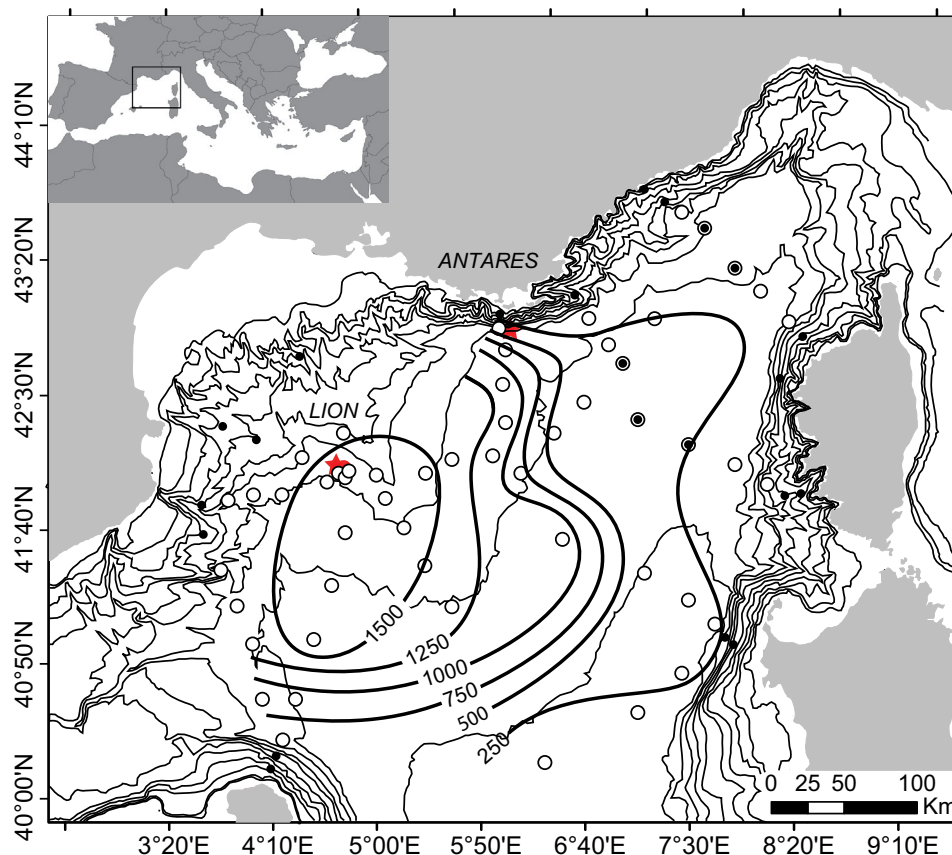
Figure 7. Map of the BNL thickness derived from the UVP measurements during DEWEX 2 cruise (April 2013). Stations marked by a white circle indicate deep stations (bottom depth > 2000 m) having anomalous profiles of suspended particulate matter concentrations characterized by significantly increasing concentrations with depth (i.e., BNL). Black donuts indicate stations where near-bottom UVP measurements were missing. Black points indicate stations having a bottom depth below 2000 m. The red stars show the position of the LION and ANTARES mooring sites.

3.1.4. The 25–27 February 2013 Event

A detailed analysis of the current and suspended particle concentration time series at the mooring site has been carried out to detect episodes of synchronous increase of current and particle concentration throughout the water column. One remarkable event was detected between the 25 and 27 February 2013 (Figure 10), exhibiting a significant increase of particles concentration at 2300 m depth following near-bottom current reaching a maximum speed of 28 cm s^{-1}. An increase in concentration also appears about 3 h later at 1000 m depth. A progressive concentration increase is visible in the following hours at depths of 500, 250, and 150 m. Such a vertical transfer implies an upward velocity of about 10 cm s^{-1}, which is consistent with the vertical velocities observed at the different levels of the mooring away from the bottom boundary layer, at a time of strong surface heat and buoyancy losses (between 400 and 800 W m^{-2} [see *Houpert et al.*, 2016]).

Between the 25 and 28 February 2013, a glider crossing the convection region observed a patch of higher turbidity between the surface and 1000 m deep, not far from the LION mooring site (Figure 11a). A good correspondence appeared between the vorticity of the water column (Figure 11b)—calculated from the glider's depth-average current—and the turbidity (Figure 11b). Turbidity significantly increased with positive vorticity (indicative of cyclonic rotation), and is homogeneous between the surface and 1000 m deep (Figure 11d).

3.2. Interannual Variability During the 2009–2015 Period
3.2.1. Time Series at the Mooring Sites

The time series of potential temperature, horizontal and vertical current speeds at different depths at the LION mooring site are depicted in Figure 12. The cooling with complete homogenization of the water column (Figure 12a) and the strong vertical current velocities (Figure 12c) observed for the winters 2010 to
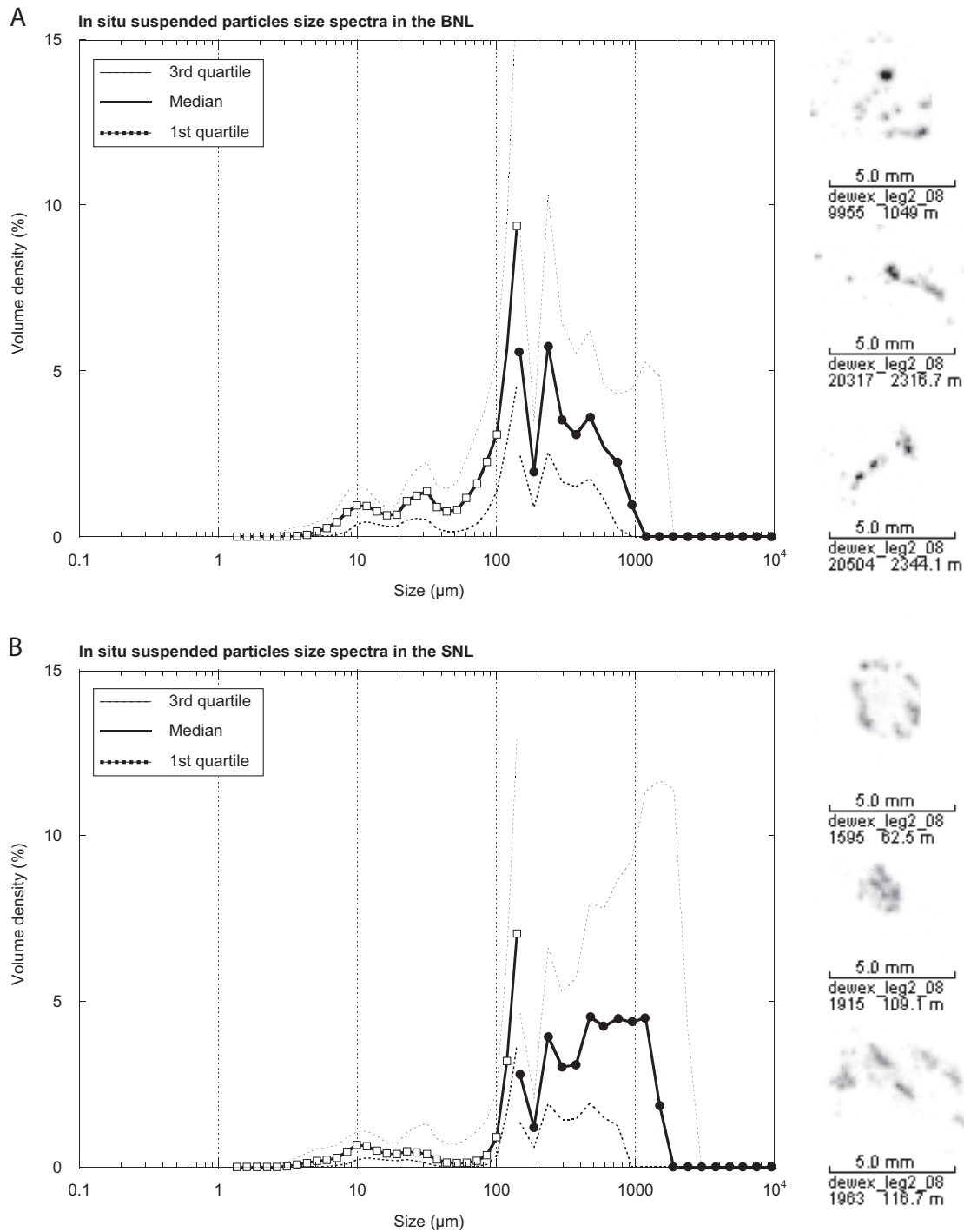
Figure 8. Size spectra of particulate matter for all deep stations (bottom depth > 2000 m) having both LISST and UVP data during the DEWEX 2 cruise (April 2013). (a) Situation in the BNL (i.e., below the clear water minimum) and (b) in the SNL (i.e., above the clear water minimum). Median (solid line), first and third quartiles (dashed lines) values are represented for each size classes. White squares and black circles represent LISST-Deep and UVP data, respectively. Thumbnails show examples large particles seen by the UVP for station 8 (presented in Figure 2).

2013 evidenced bottom-reaching open-ocean convection. For the two following winters (2014 and 2015), the convection was milder. It penetrated down to a depth comprised between 500 and 1000 m in 2014 and to more than 1000 m in 2015. The near-bottom cooling event observed during the winter 2012 results from the appearance of very cold and dense shelf water that cascaded down the slope and spread throughout the northwestern Mediterranean basin as described by *Durrieu de Madron et al.* [2013]. Years with bottom-reaching convection were also characterized by strong horizontal current speeds (peaking at
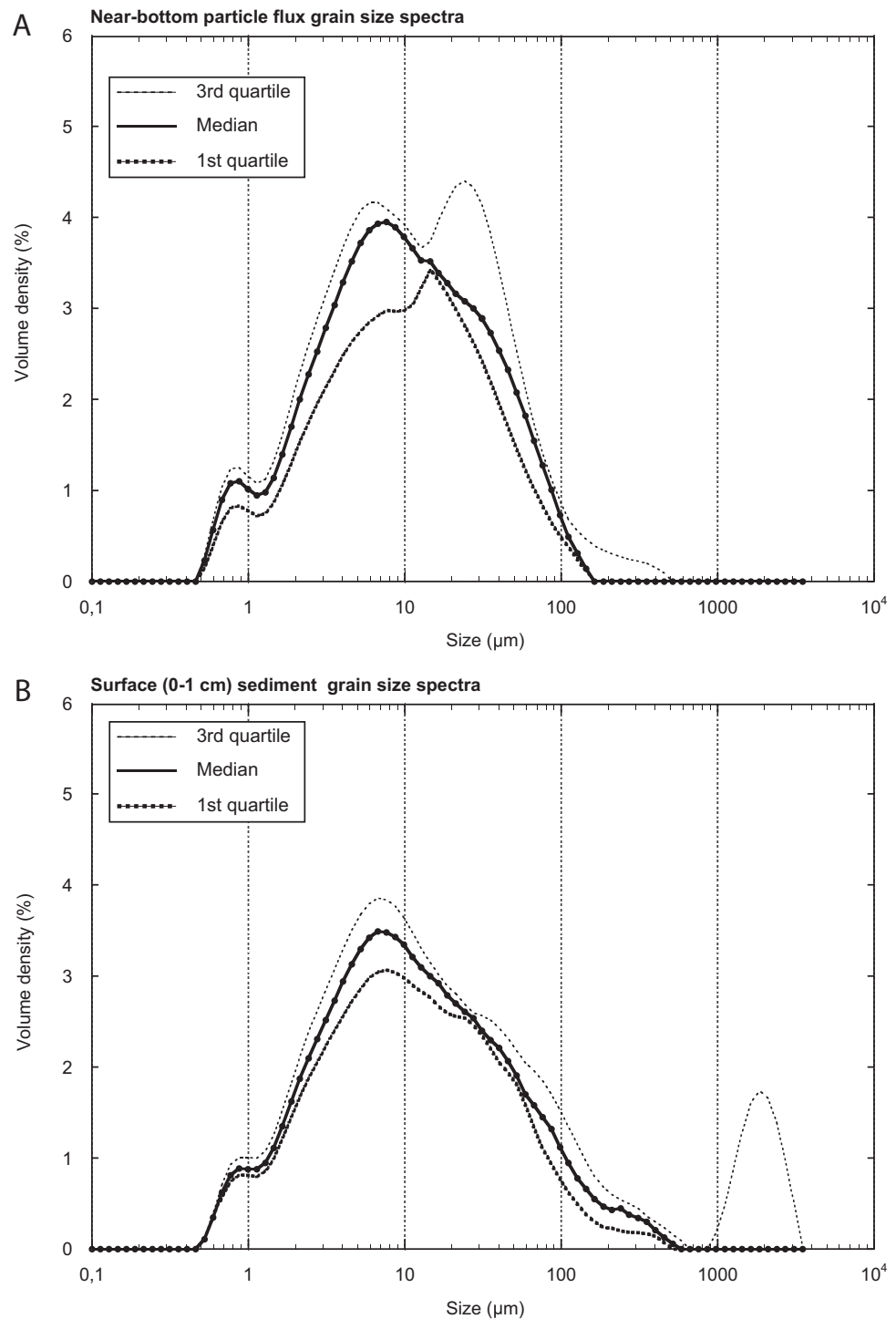
Figure 9. Size spectra of particulate matter from (a) near-bottom sediment trap and (b) surface sediment samples at the LION site in the convection region. Median (solid line), first and third quartiles (dashed lines) values are represented for each size classes. Sediment trap samples were collected on a fortnightly basis between 1 February 2013 and 31 March 2013 encompassing the very high flux period. Sediment samples are from the first centimeter of the seafloor.

around 45 cm s^{-1}) throughout the water column from late winter to late spring (Figure 12b). Both horizontal and vertical current speeds were weaker during the mild winters 2014 and 2015.

Both the near-bottom suspended particle concentration (Figure 12d) and bioluminescence (Figure 12e) showed significant increases during and after the bottom-reaching convection events. In contrast, no
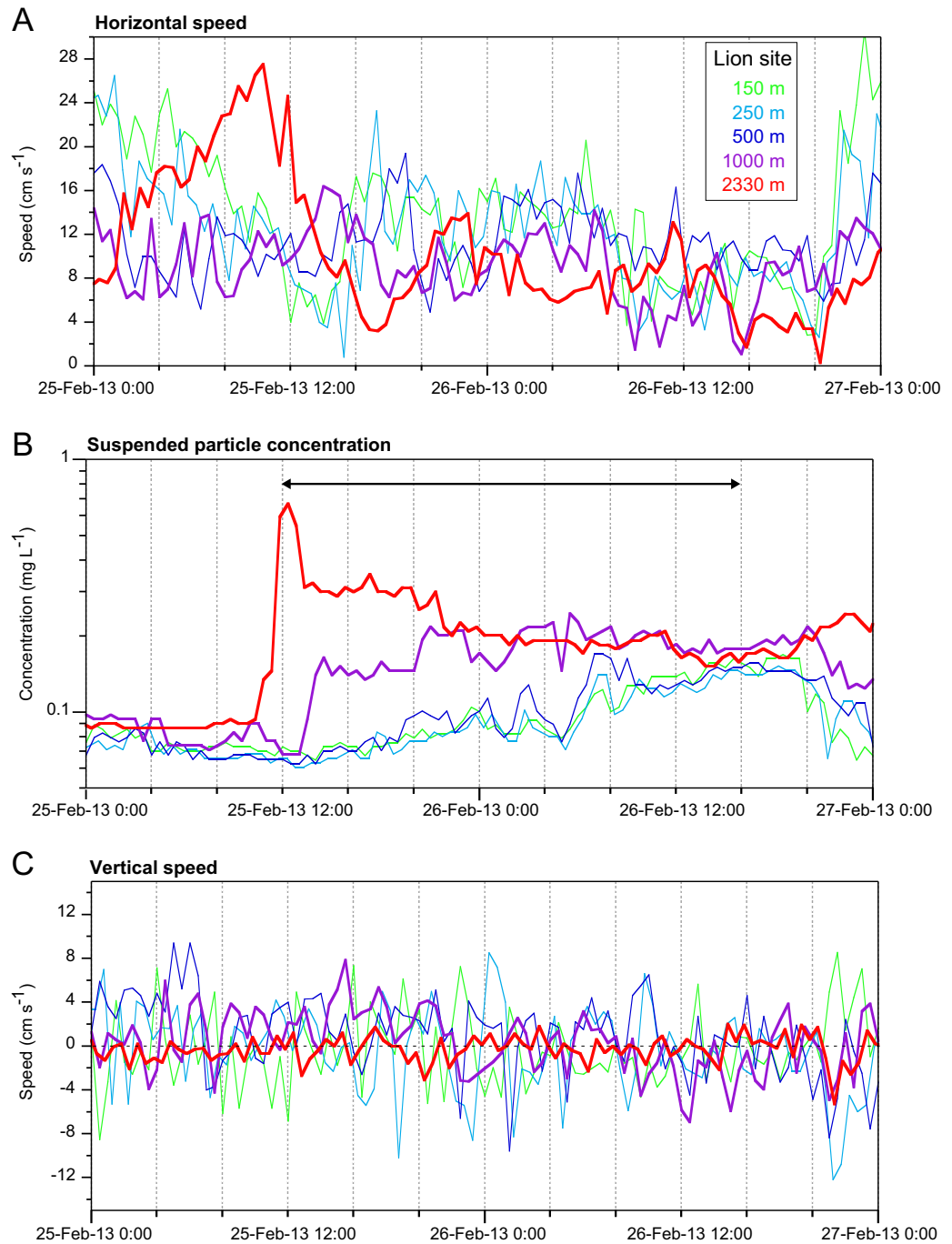
Figure 10. Temporal evolution of the (a) horizontal speed, (b) SPM concentrations, and (c) vertical speed at different levels at the LION site in the convection region between the 25 and 27 February 2013 showing the resuspension and rapid upward motion of resuspended sediment. The arrow indicates the transit time of particle concentration from the seabed to the surface.

significant increase was observed near the bottom during the winters of 2014 and 2015 while the convection did not reach the seabed. It is worthy to note that despite the increase of the horizontal current speed—with peaks up to 25 cm s^{-1}—following the spring 2015, both the near-bottom concentration of suspended particle concentration and bioluminescence activity remained at low levels. The increase of suspended particle concentration at 150 m, which is clearly visible in 2014 and 2015 but also occurred the previous years, likely resulted from the higher abundance of planktonic organisms during the spring bloom that followed the convection period [*Lavigne et al.*, 2013].
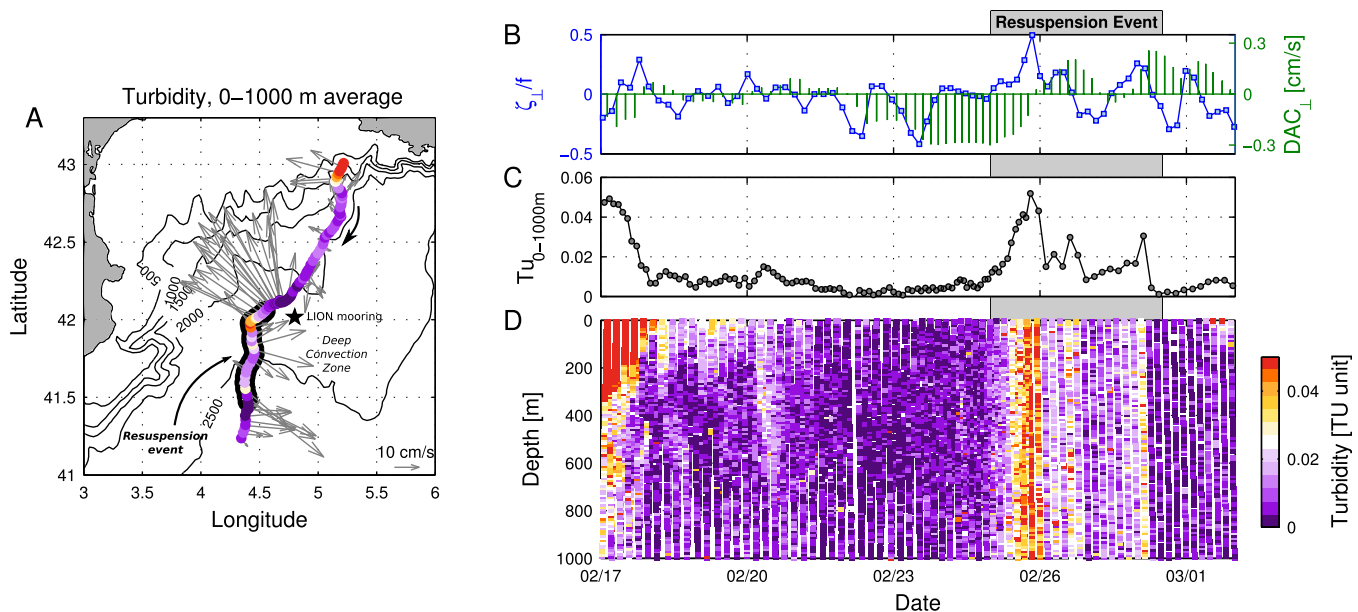
Figure 11. (a) Glider track crossing the convection region from 17 February to 2 March 2013 with the signal of average turbidity between the surface and 1000 m deep and horizontal depth-average currents. (b) Glider-based vorticity (in blue) and cross-track depth-average currents (in green) used to estimate it. (c) Turbidity signal average over the top 1000 m sampled by the glider. (D) Turbidity section measured by the glider.

3.2.2. Suspended Particles Distribution During the Summer Cruises

The suspended particles distribution of large suspended particles with respect to density observed during the MOOSE-GE summer cruises are depicted in Figure 13. Profiles for the summer 2012 and 2013 (Figures 13a and 13b), which followed bottom-reaching convection events, showed a well-defined BNL with an average CWM abundance around 15–35 particles L^{-1} and a significant increase toward the bottom, where abundance reached average values about 500 particles L^{-1} in 2012 and 100 particles L^{-1} in 2013. By contrast, profiles for the summer 2014 and 2015 (Figures 13c and 13d), which followed mild convection, were homogeneous over the whole water column with mean abundance in the range 40–70 particles L^{-1}.

4. Discussion

Various points are discussed in this section. First, we review the evidence and recurrence of deep sediment resuspension by open-ocean convection. Second, we investigate the mechanism responsible for the upward motion of suspended particulate matter and formation of BNL. Third, we consider the combined effect of convection and deep water intrusion on the fueling of the BNL. Finally, we infer possible implications on the deep pelagic ecosystem.

4.1. Evidence and Recurrence of Deep Sediment Resuspension by Bottom-Reaching Open-Ocean Convection

The results reveal several interconnected elements. First, near-bottom particle flux increased by two orders of magnitude and POC content decreased (Figure 3e) toward value measured in the surficial sediment, while near-bottom currents and suspended particle concentrations strongly increased at the end and after bottom-reaching convection periods. Second, near-bottom trap particle size spectra are very similar with the one of the surface sediment, and are mostly composed of fine and medium silts. Finally, the observed currents at 20 m above the seabed (U_{20}) up to 45 cm s^{-1} are large enough to resuspend both small and medium silts. Based on the 2009–2015 near-bottom time series, episodes of local sediment resuspension (such as the one depicted in Figure 10) appear to occur for current speed between 17 and 30 cm s^{-1}. The bed shear stress induced by these currents, $\tau_c = \rho \times U_*^2$, ranges between 0.04 and 0.13 N m^{-2} (average 0.09 ± 0.02 N m^{-2}), with the friction velocity $U_* = 0.4 \times U_{20}/\ln(Z_{20}/Z_0)$ where ρ is the water density (= 1029.12 kg m^{-3}), U_{20} is the measured velocity at $Z_{20} = 20$ m above the seabed, and Z_0 is the bottom sediment roughness set to a constant value of 5×10^{-4} m. Using this average value as critical shear stress
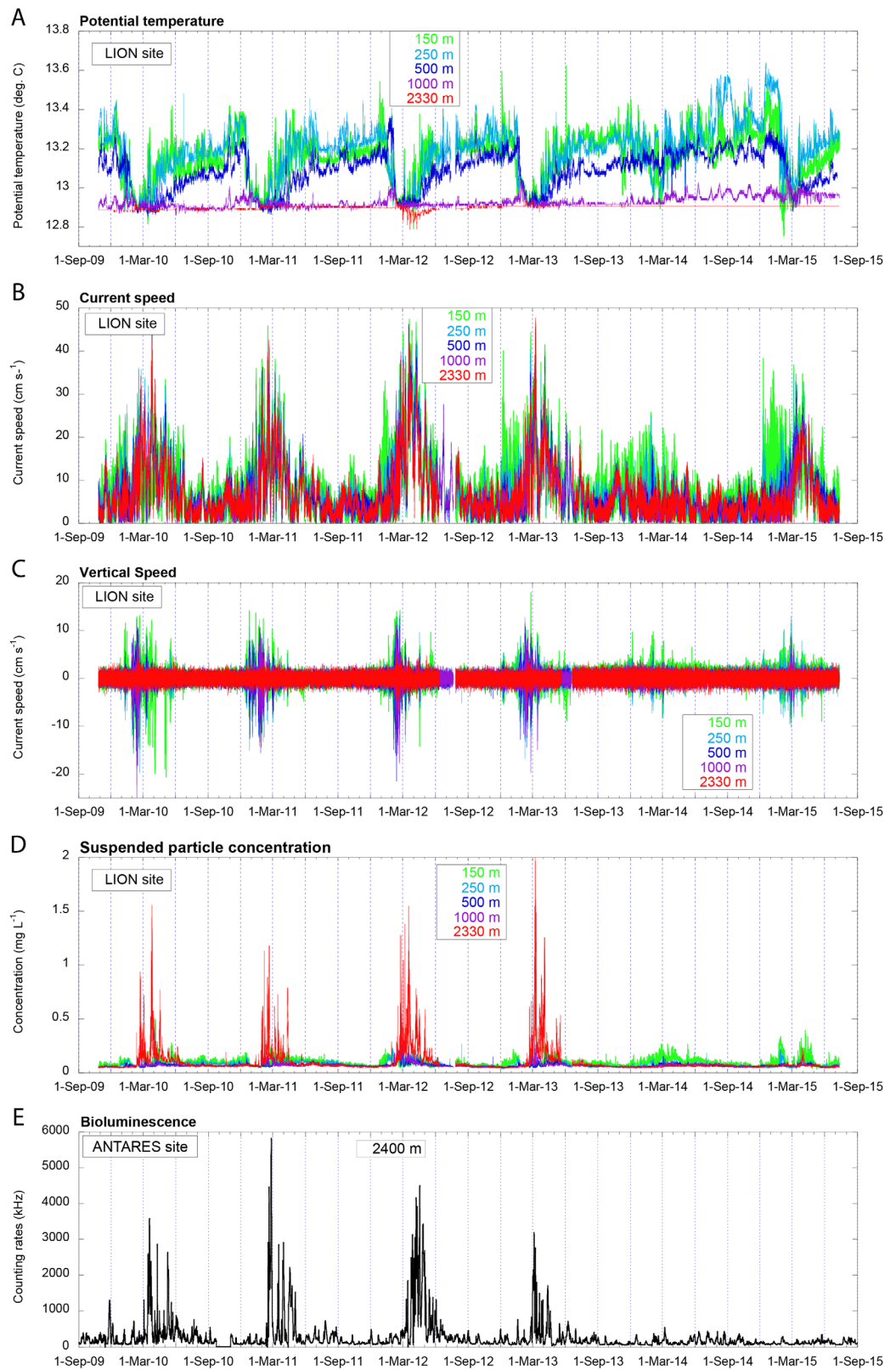
Figure 12. July 2009 to July 2015 time series of (a) potential temperature, (b) horizontal current velocities, (c) vertical current velocities, and (d) suspended particulate matter concentrations at the LION site (150, 250, 500, 1000, and 2330 m nominal depths). (e) Time series of bioluminescence at the ANTARES site (2400 m nominal depth).

Figure 13. Statistics of large particles distribution from the UVP measurements versus density for all the stations of the MOOSE-GE cruises in (a) July/August 2012, (b) June/July 2013, (c) July 2014, and (d) July 2015.

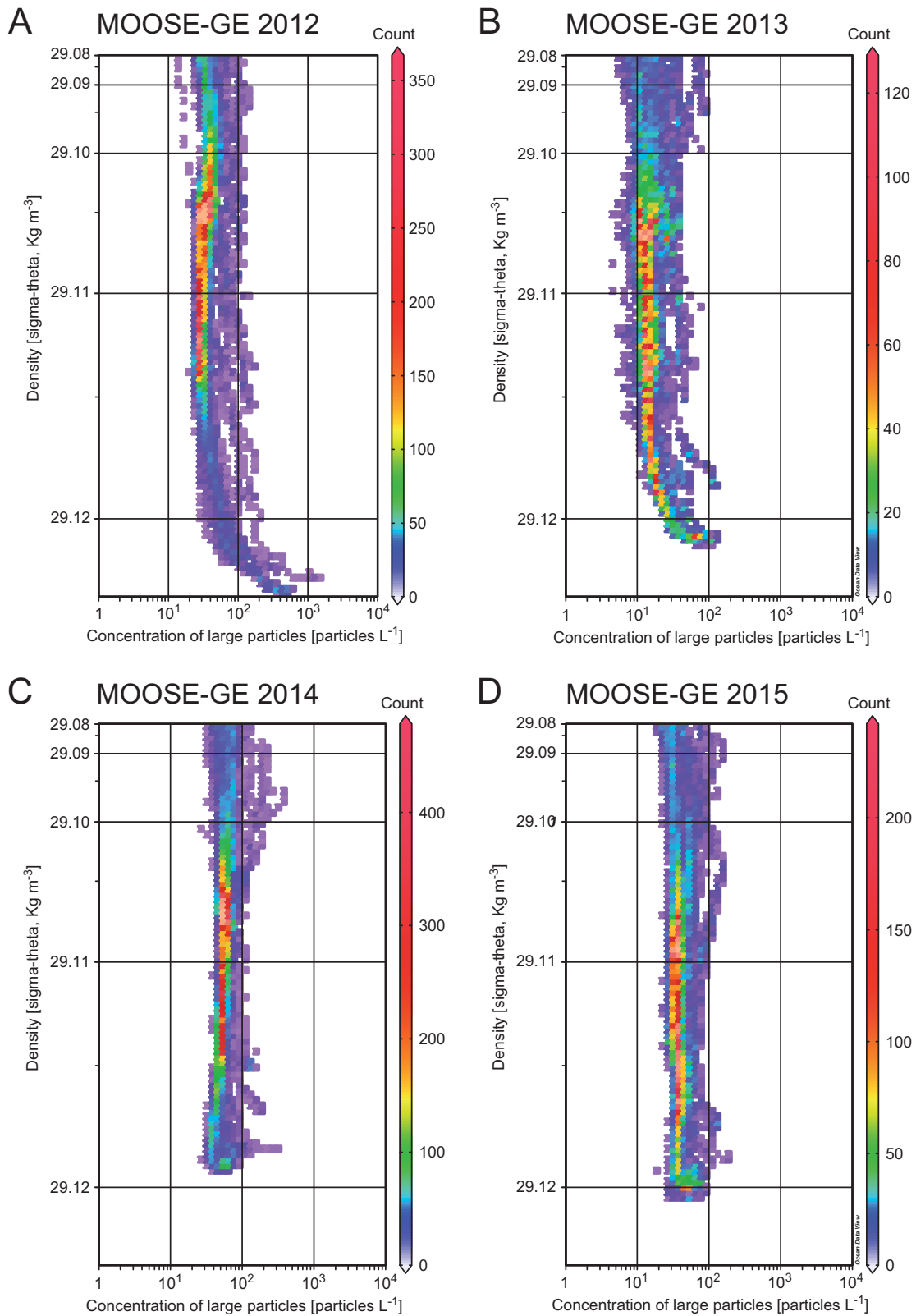for erosion (corresponding to a measured velocity of 25 cm s^{-1}), the near-bottom current speed (U_{20}) for the February–May 2013 high flux period (Figure 3b) exceeded this threshold about 8% of the time, suggesting recurrent local sediment resuspension.

From direct measurements of sediment erosion determined on cores taken between 212 and 4940 m water depth from the northeastern Atlantic continental margin, an average threshold for the erosion of the primary cohesive sediments (mean size < 30 μm) $\tau_c = 0.27 \pm 0.09$ N m^{-2} was found [*Thomsen and Gust*, 2000, Table 1]. However, they also found that cohesive sediment was covered by a thin superficial layer that was resuspended as aggregates of size >100 μm under lower shear stress ($\tau_c = 0.08 \pm 0.04$ N m^{-2}). This later value is close to the threshold we found.

Altogether, these results clearly support the conclusion that bottom-reaching convection events have an erosive impact on the deep sediment. This conclusion is in agreement with that of *Stabholz et al.* [2013]. These authors inferred that resuspension of deep sediment likely occurred in the convection region during the winter 2009 while the mixed layer reached the bottom, and not during the previous mild winter 2008 while the mixed layer barely reached 1000 m deep.

The combination of these two contiguous observing periods shows that over the last eight years, five consecutive winters from 2009 to 2013 with bottom-reaching convection, produced the resuspension of deep sediment and its redistribution through the basin and in the water column. In the absence of bottom-reaching convection, as in 2008 [*Stabholz et al.*, 2013] as well as in 2014 and 2015 (Figure 12), the near-bottom horizontal (U) and vertical currents (W), suspended particle concentrations (C), and particle fluxes (F) remained weak (U ≤ 25 cm s^{-1}; W ≤ 4 cm s^{-1}; C ≤ 0.2 mg L^{-1}; F ≤ 200 mg m^{-2} d^{-1}, respectively) and did not indicate any notable deep sediment resuspension and then did not increase the bioluminescence activity (Figure 12e).

4.2. Mechanism Responsible for the Deep Sediment Resuspension and Upward Motion of Suspended Particulate Matter

Glider measurements carried out in the end of February 2013 (Figure 11) suggest that cyclonic eddies could favor the vertical transfer of resuspended sediment in the convection zone. Those transfers are extremely fast and allow resuspended particles to reach the surface in about 1 day, as observed concomitantly at the LION mooring line (Figure 10).

In the northwestern Mediterranean Sea, cyclonic and anticyclonic submesoscale coherent vortices (SCV) are prominent features that can be formed as a result of winter convection [*Testor and Gascard*, 2003; *Testor and Gascard*, 2006]. Submesoscale eddies are presumed to result from localized mixed patches that adjusted to form persistent eddies in cyclogeostrophic balance [*McWilliams*, 1985]. The formation of cyclonic SCVs is likely favored by a winter mixed layer reaching the bottom. They are characterized by small radius (5–10 km) due to the weak stratification of the ocean deep levels and peak velocities located at great depths [*Bosse et al.*, 2016; *Damien et al.*, 2017].

Cyclonic vortices characterized by strong currents close to the bottom generate an Ekman pumping within the turbulent bottom boundary layer. Figures 11b and 11c show the modulation of the turbidity signal by the relative vorticity of barotropic currents during intense mixing event. Therefore, the Ekman pumping could be important in establishing a connection between the bottom boundary layer (rich in sediments, but with no strong vertical velocities observed) and the overlying layer where strong coherent vertical velocities are observed [*Houpert et al.*, 2016].

Open-ocean deep convection is associated with intense vertical mixing where 10 cm s^{-1} downward vertical velocities are found in small convective plumes of about 1 km in diameter, and upward vertical velocities occur around these plumes [*Marshall and Schott*, 1999; *Margirier et al.*, 2017]. In the deeper layers, the particles will rather be sensitive to the effect of individual ascending structures associated with convective plumes. It thus explains the rapid transfer in a few hours of particulate matter from the bottom to 1000 m (Figure 10b). However, it is less likely that particles will be directly transported to the surface under the effect of individual ascending structure. The slower increase of turbidity in the upper layers during the 28 h period following the episode of resuspension (Figure 10b) thus probably results from the cumulative effect of intense and quickly varying vertical water displacements (Figure 10c) that vertically diffuse sediments toward the surface. In this regard, it is interesting to see that the turbidity signal increases in the surface

layers while it decreases near the bottom (Figure 10b). These opposite trends can be interpreted as a diffusion signal with a time scale (T) of about 28 h and a thickness (H) of about 2200 m (distance between the uppermost and lowermost current meters). A vertical turbulent diffusion coefficient ($K_z \sim H^2/T$) of about 50 m^2 s^{-1} would then be associated with strong mixing phase of the deep convection.

The conceptually simplest method to measure mixing is to measure the vertical spread of a tracer over time. A 1-DV model derived from the SYMPHONIE model [*Marsaleix et al.*, 2008] was used to simulate the vertical diffusion of a particulate tracer injected at the base of a 2400 m thick water column: $\partial C/\partial t - w_s * \partial C/\partial z = K_z * (\partial^2 C)/(\partial z^2)$, where C is a tracer concentration, w_s is a constant (positive if downward) settling velocity and K_z is a constant vertical diffusivity coefficient. This equation is computed on a vertical staggered C grid using 60 equally spaced levels, a time-step of 30 s, and an initial dimensionless tracer concentration equal to 1 at the first level above the bottom and zero elsewhere. With a zero settling velocity, the theoretical vertical profile of concentration after 28 h (characteristic time from the observations) compares to the observations for a vertical diffusion coefficient starting from 20 m^2 s^{-1} (Figure 14a). Using typical flocs settling velocities from 0.01 and 10 mm s^{-1} the theoretical signal still compares to the observations, indicating that settling velocities are negligible with respect to the upward diffusion (Figure 14b). The temporal pattern (Figure 14c) further indicates that K_z of 50 m^2 s^{-1} better compares to the observations (the increase of concentration at 1000 m using $K_z = 20$ m^2 s^{-1} appears too late). This estimate of K_z of 50 m^2 s^{-1} is thus comparable to the initial scaling of vertical diffusivity. It is also consistent with the estimate based on numerical experiments on convective plumes dynamics [*Klinger et al.*, 1996]. The observed increase of particulate concentration during this event ΔC ($\approx$0.1 mg L^{-1} or 1×10^{-4} kg m^{-3}; Figure 10b) throughout a water column of height H (= 2400 m) implies, considering a seabed sediment concentration of ρs (= 500 kg m^{-3}), a seabed erosion over a thickness h = $\Delta C \times$ H/ ρs ($\approx 5 \times 10^{-4}$ m or 0.5 mm). This thickness is close to the annual sediment accumulation rate in the basin ($\leq$ 1 mm yr^{-1}) [*Durrieu de Madron et al.*, 2000].

During the summer MOOSE-GE 2012 cruise, two cyclonic SCVs were observed along the continental slope in the vicinity of the convection region [*Durrieu de Madron et al.*, 2013; *Bosse et al.*, 2016]. The vertical profiles of density and large particle abundance in an eddy identified as a cyclonic SCV by *Bosse et al.* [2016] is depicted in Figure 15. It exhibited an uplifting of the isopycnal of nearly 2000 m and a thick BNL with average particle abundance $\sim$200 particles L^{-1} (i.e., about one order of magnitude larger than the surrounding waters, except in the bottommost layer associated with newly formed deep waters and the BML). Cyclonic SCVs are long-lived features (average time life order of a year) that preserve in their core the deep waters formed during the convection and transport them over long distances [*Bosse et al.*, 2016; *Damien et al.*, 2017]. Very thick BNL of 1000–2000 m can thus be transported (and maintained by the Ekman pumping) within persistent and isolated cyclonic SCVs that could potentially wander throughout the northwestern Mediterranean basin and also to the Algerian basin. Besides, according to a numerical study by *Damien et al.* [2017], post-convective eddies can also interact with the large-scale circulation along the continental slope, and their structure is then eroded due to the frictional effects caused by the interaction with the topography and the large-scale currents. As a result of these interactions, cyclonic eddies are destroyed and their core waters gorged with suspended particle released into the currents flowing across the northern Mediterranean basin and toward the Algerian Basin.

4.3. Combined Effect of Convection and Deep Water Intrusion on the Formation of BNL

BNLs with large particle abundance higher than 100 particles L^{-1} are rather peculiar in the Mediterranean. Reference conditions collected during the BOUM cruise in summer across the eastern and western Mediterranean [*Moutin et al.*, 2012] and also in the Northern Current in the Ligurian Sea [*Stemmann et al.*, 2008] show that abundance in the entire water column below the surface layer is homogeneous and around 10–20 particles L^{-1}. This value is similar to the CWM abundance observed in 2012/2013 and also to the average abundance observed during the summer of 2014 and 2015 cruises following mild winters with no deep sediment resuspension nor lateral advection of slope sediments. It suggests that this background abundance is probably associated to the settling of biogenic particles from the surface.

Thick nepheloid layers in the Gulf of Lions have been already described [*Béthoux et al.*, 2002; *Puig et al.*, 2013]. In the latter study, the authors reviewed the interannual variability of the BNL between 1998 and 2011. They related the occurrence of these BNL primarily to severe and massive dense shelf water cascading events (such as those of winter 2012, but also the winters 1999 [*Béthoux et al.*, 2002], 2005 [*Canals et al.*, 2006], and 2006
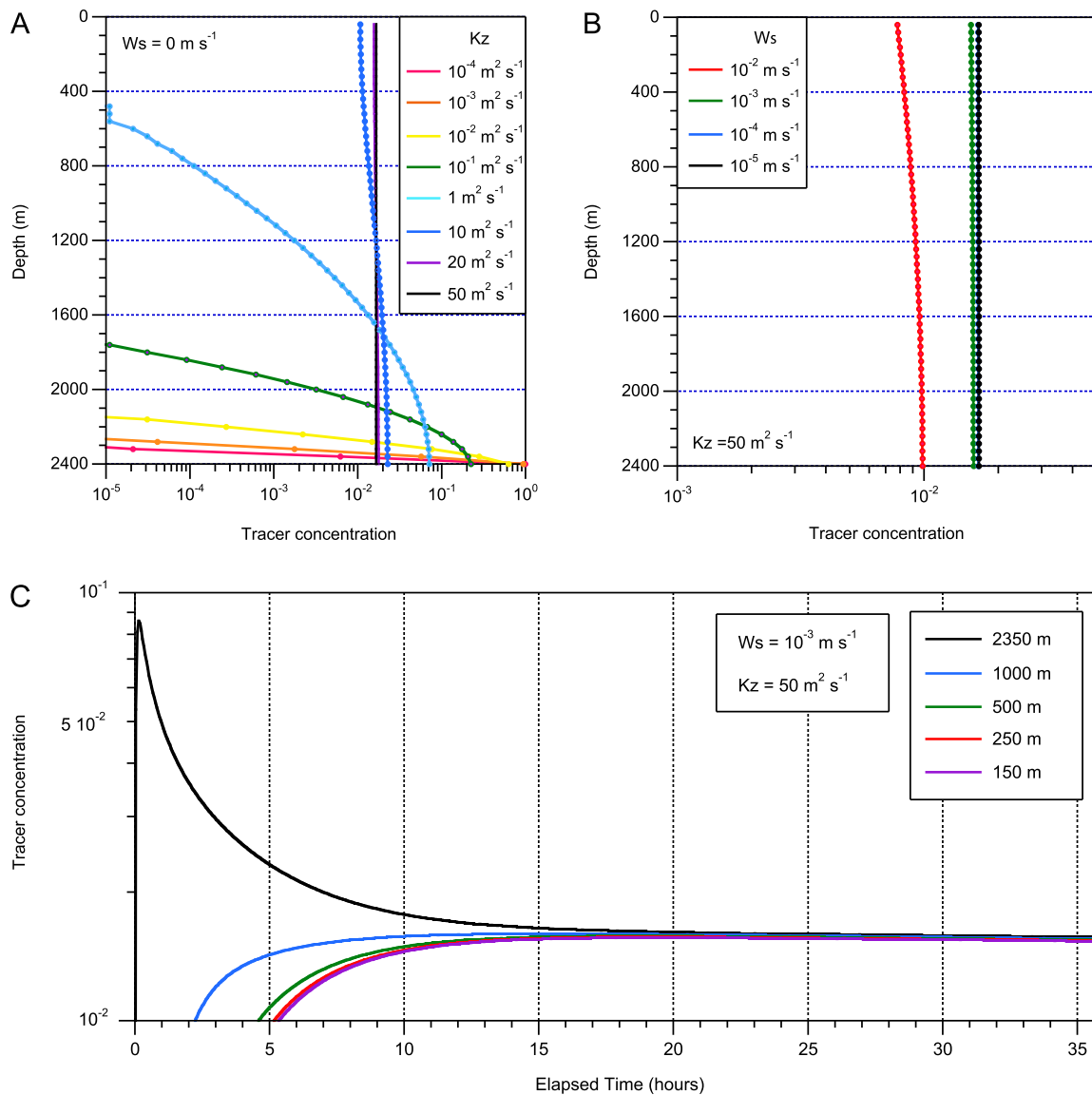
Figure 14. Results of the 1-DV model. (a) Vertical profile of tracer concentration after 28 h for different constant vertical diffusion coefficients from 1×10^{-4} to 50 m^2 s^{-1}. (b) Vertical profile of tracer concentration after 28 h for different vertical settling velocities and for a constant vertical diffusion coefficients 50 m^2 s^{-1}. (c) Temporal evolution of a tracer concentration at different depths corresponding to the moored instruments for a constant vertical diffusion coefficient of 50 m^2 s^{-1} and a settling velocity of 1×10^{-3} m s^{-1}.

[*Palanques et al.*, 2012]), but nevertheless suggested the potential effect of open-sea convection. It is obvious that deep dense shelf water cascading can transport resuspended sediment eroded along the continental slope by very strong descending currents (>1.0 m s^{-1}) [*Palanques et al.*, 2012; *Durrieu de Madron et al.*, 2013]. However, we believe that concomitant bottom-reaching open-sea convection and the subsequent spreading of the newly formed deep waters are the main mechanisms responsible for the formation of this thick BNL.

At the end of the strong bottom-reaching mixing period, horizontal currents increase due to the spreading of the newly formed deep water and the restratification of the ambient water masses, and occasionally exceed the critical speed threshold for erosion. During this period vertical currents are still strong and resuspended sediment is likely to be entrained vertically in the homogeneous water column (see the previous section). During the following spreading phase, the dense newly formed deep waters propagate swiftly throughout the basin, and a significant proportion is also trapped within submesoscale coherent vortices (SVC) [*Testor and Gascard*, 2006; *Bosse et al.*, 2016]. The strong and barotropic horizontal currents up to 45 cm s^{-1} that lasted from March until May (Figures 3b and 12b) can erode deep sediments. However, the weakness of the vertical displacements outside the strong mixing period (Figures 3c and 12c) hinders the
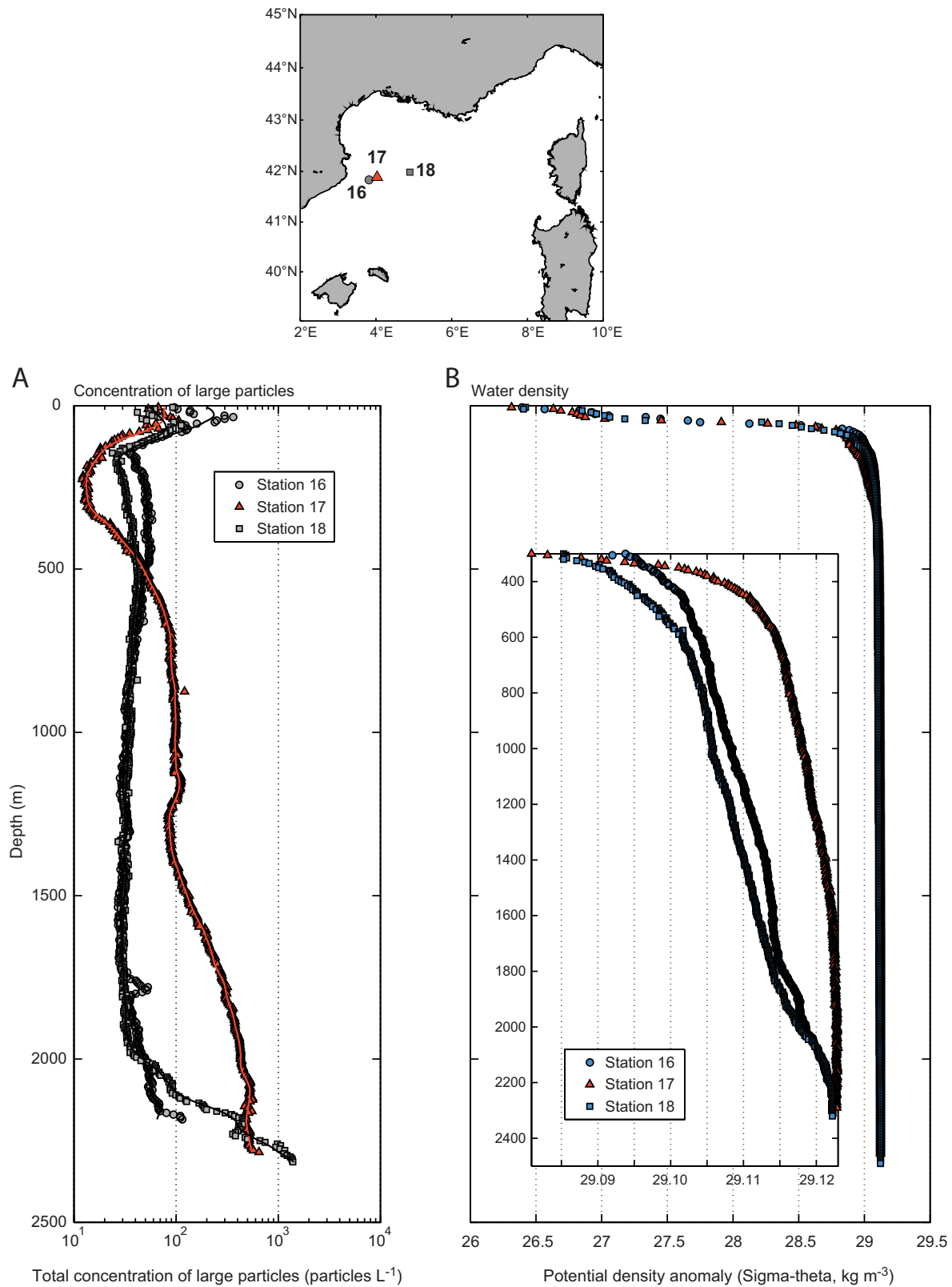
Figure 15. Profiles of (a) large particle concentration (UVP measurements) and (b) potential density anomaly for 3 close and consecutive stations the Gulf of Lion basin collected during the MOOSE-GE 2012 cruise in July 2012. The inset shows a zoom of the density profiles below 300 m of depth. The thick denser and particle-rich anomalies observed for station 17 (red triangles) were sampled within a cyclonic submesoscale coherent vortex.

upward propagation of the resuspended particles that stay mainly confined to the BML, and provoke the further near-bottom increase of suspended particle concentration observed on most of the deep stations in April 2013 (Figure 6) and also in July 2012 (Figure 4).

Hence, deep dense shelf water cascading that consistently coincides with intense bottom-reaching convection events is believed to contribute to the feeding of the BNL in the basin by conveying additional suspended particles from the slope during the mixing period, and by further resuspending deep sediment during the spreading phase as dense shelf water forms a distinct bottom water mass under the dense water layer issued from the open-ocean convection [*Durrieu de Madron et al.*, 2013]. This was the case during the winters of 1999, 2005, 2006, and 2012.

Profiles of large particles abundance observed during the 2014 and 2015 summer cruises do not show any BNL (Figures 13c and 13d), and profiles are nearly homogeneous with low abundance (about few tens of particles L^{-1}) throughout the water column. The winters of 2014 and 2015 were less rigorous than in previous years, and the mixing only reached intermediate depths (around 500 m in 2014 and 1000 m in 2015). This suggests that in the absence of bottom-reaching convection and deep cascading, the deep layer of the basin remains basically free of resuspended particles. Moreover, since the BNLs formed during the winter/spring of 2012 and 2013 were not visible the following year, it is believed that BNLs last less than a year.

4.4. Implication for the Deep Pelagic Ecosystem

There is indeed evidence [see *Séverin et al.*, 2017] that nutrients concentrations are altered by the resuspension of deep sediment. *Séverin et al.* [2017] showed that during the winter cruise (DEWEX 1), in the absence of enhanced primary production, N and P concentrations for fully mixed stations are slightly larger than for stations where the mixing only affects part of the water column. This is notably expressed in the strong reduction of the N/P stoichiometric ratio. While the latter stations show minimum and homogeneous large particles abundance throughout the water column, the former stations present a weak BNL indicative of the beginning of sediment resuspension and preferential P release.

Deep-sea bioluminescence is commonly viewed as an expression of abundance and adaptation of meso-pelagic and bathy-pelagic organisms to their environment. Recently, S. Martini and S. Haddock (personal communication, 2016) demonstrated that around 70% of organisms in the whole water column are able to emit light. The record of light intensity at the nearby ANTARES site (Figure 3f) shows that during winters with bottom-reaching convection, near-bottom bioluminescence strongly increases between March and May (and even June in 2012 following the winter with strong open-sea convection and dense shelf water cascading) from background values of few hundreds of kHz to peaks of several thousands of kHz. For the winters of 2014 and 2015, with milder convection intensity and the absence of significant sediment resuspension, the bioluminescence remains low. This result confirms the observations of *Tamburini et al.* [2013], who observed a similar response of the bioluminescence during the strong 2009 and 2010 winters mixing. While bioluminescence often relates to the sole current-induced effect (i.e., reaction of organisms to impacts on the PMTs or enhanced turbulent motion in the wakes of the PMTs), *Martini et al.* [2014] demonstrated that the 2009 and 2010 event of high-intensity bioluminescence was also correlated to the spreading of newly formed deep water. *Tamburini et al.* [2013] hypothesized that this new water likely fuels deep-sea biological activity and, therefore, further increase bioluminescence by conveying dissolved and particulate organic matter issued both from the productive surface layer as well as from the eroded deep sediment.

Our results indicate that the massive near-bottom POC flux (74 mg m^{-2} d^{-1} on average) linked to sediment resuspension is comparable to the maximum near-bottom POC fluxes (47 mg m^{-2} d^{-1}) linked to the Spring planktonic bloom measured in the same region during the winter 2008, which was a mild winter with no bottom-reaching convection [*Stabholz et al.*, 2013]. Thus POC fluxes issued from the resuspension of sediment during bottom-reaching convection events are indeed likely to significantly contribute to the fueling the deep pelagic ecosystems. They also suggest that such an enhanced biological activity is not restricted to the bottom layer, where bioluminescence records are made, but possibly to a significant part of the water column corresponding to the thickness of the BNL. Besides, as shown by observations of thermohaline anomalies [*Béthoux et al.*, 2002; *Schroeder et al.*, 2008] and turbidity anomalies [*Puig et al.*, 2013], as well as numerical simulations [*Beuvier et al.*, 2012], the deep water formed in the Gulf of Lions during severe winters is likely to spread rapidly over large distance and fill most of the western Mediterranean basin within a year. Such basin wide extension of newly formed deep water, enriched in particles and associated

biogeochemical elements, is hence believed to be capable of impacting efficiently the western Mediterranean deep pelagic ecosystem.

5. Conclusions

The following conclusions can be drawn from these pluriannual observations in the Gulf of Lions:

1. During the September 2009 to September 2015 period, winter open-ocean convection reaching the bottom (between 2000 and 2500 m deep) occurred for 4 winters in succession (from 2010 to 2013). During these severe winters, near-bottom horizontal currents that take place at the end of the mixing phase and particularly during the spreading phase are able to resuspend local sediment. The critical bed shear stress is estimated to about 0.09 ± 0.02 N m^{-2}.

2. Sediment resuspension and upward transport start to take place at the end of the bottom-reaching mixing period, while horizontal currents get strong enough to erode superficial fine sediment and vertical currents are still significant. Cyclonic SCVs, which form during the winter convection, appear to favor the upward motion of the resuspended sediment throughout the water column, and thus contribute to the formation of a thick BNL that may reach the sea surface.

3. Resuspension of local sediment is maximum during the subsequent spreading phase as horizontal current are maximum and reach velocities well over the resuspension threshold of fine sediments. However, upward transport is limited to the bottom layer as vertical currents vanished, and resuspended sediment remains confined within the bottom most part of the BNL that is clearly associated to the BML.

4. The BNL is clearly visible from either light attenuation or digital particle imaging measurements. It is primarily composed of aggregates between 100 and 1000 μm in diameter, probably composed of fine silts. Following the bottom-reaching mixing period, the BNL is thicker in the convection region (up to 2000 m) and shrinks rapidly in the periphery. Large particle abundance at CWM is one-to-two orders of magnitude lower than close to the seabed. The BNL is still visible the next summer over the whole northwestern Mediterranean basin, especially within the core of cyclonic SCV. The BNL is believed to last less than a year.

5. The hydrodynamical and biogeochemical alteration of the environmental conditions, appear to trigger a significant response of the deep-sea biological activity as seen by bioluminescent intensity.

6. Finally, this study confirms and emphasizes the effect of bottom-reaching open ocean convection and eddy activity in the Gulf of Lions as effective mechanisms to resuspend deep sediment and form thick BNLs. It adds up to the impact of deep dense shelf water cascading, as in 2005 and probably also 2012 that supplies an extra amount of fine sediment from the shelf and slope. The synergetic impact of both mechanisms is very important for the genesis of large turbid anomalies in the basin, but bottom-reaching open-sea convection appears to be able to feed and maintain the BNL in the absence of deep cascading. This process comes in addition to other mechanisms of high kinetic energy (western boundary currents, eddy, internal tides, benthic storms) responsible of deep sediment resuspension and BNL formation that have been evidenced in other oceanic regions.

Appendix A

A. Albert[1], M. André[2], M. Anghinolfi[3], G. Anton[4], M. Ardid[5], J.-J. Aubert[6], T. Avgitas[7], B. Baret[7], J. Barrios-Marti[8], S. Basa[9], V. Bertin[6], S. Biagi[10], R. Bormuth[11,12], S. Bourret7, M.C. Bouwhuis[11], R. Bruijn[11,13], J. Brunner[6], J. Busto[6], A. Capone[14,15], L. Caramete[16], J. Carr[6], S. Celli[14,15,17], T. Chiarusi[18], M. Circella[19], J.A.B. Coelho[7], A. Coleiro[7], R. Coniglione[10], H. Costantini[6], P. Coyle[6], A. Creusot[7], A. Deschamps[20], G. De Bonis[14,15], C. Distefano[10], I. Di Palma[14,15], C. Donzaud[7,21], D. Dornic[6], D. Drouhin[1], T. Eberl[4], I. El Bojaddaini[22], D. Elsässer[23], A. Enzenhöfer[6], I. Felis[5], L.A. Fusco[18,24], S. Galatà[7], P. Gay[25,7],V. Giordano[26], H. Glotin[27,28], T. Grégoire[7], R. Gracia Ruiz[7], K. Graf[4], S. Hallmann[4], H. van Haren[29], A.J. Heijboer[11], Y. Hello[20], J.J. Hernandez-Rey[8], J.Hößl[4], J. Hofestädt[4], C. Hugon[3,30], G. Illuminati[8], C.W James[4], M. de Jong[11,12], M. Jongen[11], M. Kadler[23], O. Kalekin[4], U. Katz[4], D. Kießling[4], A. Kouchner[7,28], M. Kreter[23], I. Kreykenbohm[31], V. Kulikovskiy[6,32], C. Lachaud[7], R. Lahmann[4], D. Lefèvre[33], E. Leonora[26,34], M. Lotze[8], S. Loucatos[35,7], M. Marcelin[9], A. Margiotta[18,24], A. Marine-Illi[36,37], J.A. Martínez-Mora[5], A. Mathieu[6], R. Mele[38,39], K. Melis[11], T. Michael[11], P. Migliozzi[38], A. Moussa[22], E. Nezri[9], G.E. Păvălaş[16], C. Pellegrino[18,24], C. Perrina[14,15], P. Piattelli[10], V. Popa[16], T. Pradier[40], L. Quinn[6], C. Racca[1], G. Riccobene[10], A. Sánchez-Losa[19], M. Saldaña[5], I. Salvadori[6], D. F. E. Samtleben[11,12], M. Sanguineti[3,30], P. Sapienza[10], F. Schüssler[35], C. Sieger[4], M. Spurio[18,24], Th. Stolarczyk[35], M. Taiuti[3,30], Y. Tayalati[41], A.

Trovato[10], D. Turpin[6], C. Tönnis[8], B. Vallage[35,7], C. Vallée[6], V. Van Elewyck[7,28], F . Versari[18,24], D. Vivolo[18,24], A. Vizzoca[14,15], J. Wilms[31], J.D. Zornoza[8], J. Zúñiga[8]

[1]GRPHE - Université de Haute Alsace - Institut universitaire de technologie de Colmar, France [2]Technical University of Catalonia, Laboratory of Applied Bioacoustics, Barcelona, Spain [3]INFN - Sezione di Genova, Italy [4]Friedrich-Alexander-Universität Erlangen-Nürnberg, Erlangen Centre for Astroparticle Physics, Erlangen, Germany [5]Institut d'Investigacio per a la Gestio Integrada de les Zones Costaneres (IGIC) - Universitat Politecnica de València. Gandia, Spain [6]CPPM, Aix Marseille University, CNRS/IN2P3, Marseille, France [7]APC, Université Paris Diderot, CNRS/IN2P3, CEA/IRFU, Observatoire de Paris, Sorbonne Paris Cité, Paris, France [8]Instituto de Fisica Corpuscular, CSIC - Universitat de València) Valencia, Spain [9]Laboratoire d'Astrophysique de Marseille, Marseille, France [10]INFN - Laboratori Nazionali del Sud, Catania, Italy [11]NIKHEF, Amsterdam, The Netherlands [12]Huygens-Kamerlingh Onnes Laboratorium, Universiteit Leiden, The Netherlands [13]Universiteit van Amsterdam, Instituut voor Hoge-Energie Fysica, Amsterdam, The Netherlands [14]INFN - Sezione di Roma, Roma, Italy [15]Dipartimento di Fisica dell'Università La Sapienza, Roma, Italy [16]Institute for Space Science, Măgurele, Romania,[17]Gran Sasso Science Institute, L'Aquila, Italy [18]INFN - Sezione di Bologna, Bologna, Italy [19]INFN - Sezione di Bari, Bari, Italy [20]GEO-AZUR, UCA, CNRS, IRD, Observatoire de la Côte d'Azur, Sophia Antipolis, France [21]Université Paris-Sud, Orsay, France [22]University Mohammed I, Laboratory of Physics of Matter and Radiations, Oujda, Morocco [23]Institut für Theoretische Physik und Astrophysik, Universität Würzburg, Würzburg, Germany [24]Dipartimento di Fisica e Astronomia dell'Università, Bologna, Italy [25]Laboratoire de Physique Corpusculaire, Université Blaise Pascal, CNRS/IN2P3, Clermont-Ferrand, France [26]INFN - Sezione di Catania, Catania, Italy [27]LSIS, Aix Marseille Université, CNRS, ENSAM, Marseille; Université de Toulon CNRS, La Garde, France [28]Institut Universitaire de France, Paris, France [29]Royal Netherlands Institute for Sea Research, Den Hoorn Texel, The Netherlands [30]Dipartimento di Fisica dell'Università, Genova, Italy [31]Remeis-Sternwarte and ECAP, Universität Erlangen-Nürnberg, Bamberg, Germany [32]Moscow State University, Skobeltsyn Institute of Nuclear Physics, Moscow, Russia [33]Mediterranean Institute of Oceanography, Aix-Marseille University, CNRS/INSU, IRD, Marseille, Université du Sud Toulon-Var, La Garde, France [34]Dipartimento di Fisica ed Astronomia dell'Università, Catania, Italy [35]Direction des Sciences de la Matière - Institut de recherche sur les lois fondamentales de l'Univers - Service de Physique des Particules, CEA Saclay, Gif-sur-Yvette, France [36]INFN - Sezione di Pisa, Pisa, Italy [37]Dipartimento di Fisica dell'Università, Pisa, Italy [38]INFN - Sezione di Napoli, Napoli, Italy [39]Dipartimento di Fisica dell'Università Federico II di Napoli, Napoli, Italy [40]IPHC Université de Strasbourg, CNRS, Strasbourg, France [41]University Mohammed V in Rabat, Faculty of Sciences, Rabat, Morocco

References

Ageron, M., et al. (2011), ANTARES: The first undersea neutrino telescope, *Nucl. Instrum. Methods Phys. Res., Sect. A*, *656*, 11–38.

Agrawal, Y. C., and H. C. Pottsmith (2000), Instruments for particle size and settling velocity observations in sediment transport, *Mar. Geol.*, *168*(1–4), 89–114.

Auffret, G., A. Khripounoff, and A. Vangriesheim (1994), Rapid post-bloom resuspension in the northeastern Atlantic, *Deep Sea Res., Part I*, *41*(5), 925–939.

Baker, E. T. (1976), Temporal and spatial variability of the bottom nepheloid layer over a deep-sea fan, *Mar. Geol.*, *21*(2), 67–79.

Béthoux, J. P., X. Durrieu de Madron, F. Nyffeler, and D. Taillez (2002), Deep water in the western Mediterranean: Peculiar 1999 and 2000 characteristics, shelf formation hypothesis, variability since 1970 and geochemical inferences, *J. Mar. Syst.*, *33–34*, 117–131.

Beuvier, J., K. Béranger, C. Lebeaupin Brossier, S. Somot, F. Sevault, Y. Drillet, R. Bourdallé-Badie, N. Ferry, and F. Lyard (2012), Spreading of the Western Mediterranean Deep Water after winter 2005: Time scales and deep cyclone transport, *J. Geophys. Res.*, *117*, C07022, doi:10.1029/2011JC007679.

Biscaye, P. E., and S. L. Eittreim (1977), Suspended particulate loads and transports in the nepheloid layer of the abyssal Atlantic Ocean, *Mar. Geol.*, *23*, 155–172.

Bosse, A., P. Testor, L. Mortier, L. Prieur, V. Taillandier, F. d'Ortenzio, and L. Coppola (2015), Spreading of Levantine Intermediate Waters by submesoscale coherent vortices in the northwestern Mediterranean Sea as observed with gliders, *J. Geophys. Res. Oceans*, *120*, 1599–1622, doi:10.1002/2014JC010263.

Bosse, A., et al. (2016), Scales and dynamics of submesoscale coherent vortices formed by deep convection in the northwestern Mediterranean Sea, *J. Geophys. Res. Oceans*, *121*, 7716–7742, doi:10.1002/2016JC012144.

Bourrin, F., G. Many, X. Durrieu de Madron, J. Martín, P. Puig, L. Houpert, P. Testor, S. Kunesch, K. Mahiouz, and L. Béguery (2015), Glider monitoring of shelf suspended particle dynamics and transport during storm and flooding conditions, *Cont. Shelf Res.*, *109*(10), 135–149.

Canals, M., P. Puig, X. Durrieu de Madron, S. Heussner, A. Palanques, and J. Fabrès (2006), Flushing submarine canyons, *Nature*, *444*, 354–357.

Conan, P. (2013), *DEWEX-MERMEX 2013 LEG2*, RV Le Suroît, doi:10.17600/13020030. [Available at http://campagnes.flotteoceanographique.fr/campagnes/13020030/fr/.]

Costantini, H., and the ANTARES Collaboration (2010), The Antares deep-sea neutrino telescope: Operation and calibration, *Nucl. Instrum. Methods Phys. Res., Sect. A*, *639*, 26–29.

Damien, P., A. Bosse, P. Testor, P. Marsaleix, and C. Estournel (2017), Modeling post-convective submesoscale coherent vortices in the northwestern Mediterranean Sea, *J. Geophys. Res. Oceans*, in press.

Donoso, K., F. Carlotti, M. Pagano, B. Hunt, R. Escribano, and L. Berline (2017), Zooplankton community response to the winter 2013 deep convection process in the NW Mediterranean Sea, *J. Geophys. Res. Oceans*, in press.

Durrieu de Madron, X., A. Abassi, S. Heussner, A. Monaco, J.-C. Aloisi, O. Radakovitch, P. Giresse, R. Buscail, and P. Kerhervé (2000), Particulate matter and organic carbon budgets for the Gulf of Lions (NW Mediterranean), *Oceanol. Acta*, *23*(6), 717–730.

Durrieu de Madron, X., et al. (2013), Interaction of dense shelf water cascading and open-sea convection in the Northwestern Mediterranean during winter 2012, *Geophys. Res. Lett.*, *40*, 1379–1385, doi:10.1002/grl.50331.

Eittreim, S., P. E. Biscaye, and A. Amos (1975), Benthic nepheloid layers and the Ekman thermal pump, *J. Geophys. Res.*, *80*, 5061–5067.

Eittreim, S., E. M. Thorndike, and L. Sullivan (1976), Turbidity distribution in the Atlantic Ocean, *Deep Sea Res. Oceanogr. Abstr.*, *23*(12), 1115–1127.

Ewing, M., S. L. Eittreim, J. I. Ewing, and X. Le Pichon (1971), Sediment transport and distribution in the Argentine Basin. 3. Nepheloid layer and processes of sedimentation, *Phys. Chem. Earth*, *8*, 49–77.

Feely, R. A. (1975), Major-element composition of the particulate matter in the near-bottom nepheloid layer of the Gulf of Mexico, *Mar. Chem.*, *3*(2), 121–156.

Font, J., P. Puig, J. Salat, A. Palanques, and M. Emelianov (2007), Sequence of hydrographic changes in NW Mediterranean deep water due to the exceptional winter of 2005, *Sci. Mar.*, *71*(2), 339–346.

Gardner, W. D., and L. G. Sullivan (1981), Benthic storms: Temporal variability in a deep-ocean nepheloid later, *Science*, *2013*(4505), 329–331.

Gardner, W. D., J. B. Southard, and C. D. Hollister (1985), Sedimentation, resuspension and chemistry of particles in the northwest Atlantic, *Mar. Geol.*, *65*, 199–242.

Gardner, W. D., B. E. Tucholke, M. J. Richardson, and P. E. Biscaye (2017), Benthic storms, nepheloid layers, and linkage with upper ocean dynamics in the western North Atlantic, *Mar. Geol.*, doi:10.1016/j.margeo.2016.12.012, in press.

Gartner, J. W. (2004), Estimating suspended solids concentrations from backscatter intensity measured by acoustic Doppler current profiler in San Francisco Bay, California, *Mar. Geol.*, *211*, 169–187.

Gostiaux, L., and H. Van Haren (2010), Extracting meaningful information from uncalibrated backscattered echo intensity data, *J. Atmos. Oceanic Technol.*, *27*, 943–949.

Gross, T. F., A. J. Williams III, and A. R. M. Newell (1988), A deep-sea sediment transport storm, *Nature*, *331*, 518–521, doi:10.1038/331518a0.

Heussner, S., C. Ratti, and J. Carbonne (1990), The PPS 3 time series sediment traps and the trap sample processing techniques used during the ECOMARGE experiment, *Cont. Shelf Res.*, *10*, 943–958.

Heussner, S., X. Durrieu de Madron, A. Calafat, M. Canals, J. Carbonne, N. Delsaut, and G. Saragoni (2006), Spatial and temporal variability of downward particle fluxes on a continental slope: Lessons from an 8-yr experiment in the Gulf of Lions (NW Mediterranean), *Mar. Geol.*, *234*, 63–92.

Houpert, L., et al. (2016), Observations of open-ocean deep convection in the northwestern Mediterranean sea: Seasonal and interannual variability of mixing and deep water masses for the 2007–2013 period, *J. Geophys. Res. Oceans*, *121*, 8139–8171, doi:10.1002/2016JC011857.

Hunkins, K., E. M. Thorndike, and G. Mathieu (1969), Nepheloid layers and bottom currents in the Arctic Ocean, *J. Geophys. Res.*, *74*, 6995–7008.

Klinger, B. A., J. Marshall, and U. Send (1996), Representation of convective plumes by vertical adjustment, *J. Geophys. Res.*, *101*, 18,175–18,182.

Lavigne, H., F. D'Ortenzio, C. Migon, H. Claustre, P. Testor, M. Ribera d'Alcala, R. Lavezza, L. Houpert, and L. Prieur (2013), Enhancing the comprehension of mixed layer depth control on the Mediterranean phytoplankton phenology, *J. Geophys. Res. Oceans*, *118*, 3416–3430, doi:10.1002/jgrc.20251.

Margirier, F., et al. (2017), Description of convective plumes associated with deep convection from glider measurements, *J. Geophys. Res. Oceans*, in press.

Marsaleix, P., F. Auclair, J. W. Floor, M. J. Herrmann, C. Estournel, I. Pairaud, and C. Ulses (2008), Energy conservation issues in sigma-coordinate free-surface ocean models, *Ocean Modell.*, *20*, 61–89, doi:10.1016/j.ocemod.2007.07.005.

Marshall, J., and F. Schott (1999), Open-ocean convection: Observations, theory, and models, *Rev. Geophys.*, *37*(1), 1–64.

Martini, S., D. Nerini, and C. Tamburini (2014), Relation between deep bioluminescence and oceanographic variables: A statistical analysis using time-frequency decompositions, *Prog. Oceanogr.*, *127*, 117–128.

McCave, I. N. (1983), Particulate size spectra, behavior, and origin of nepheloid layers over the Nova Scotian Continental Rise, *J. Geophys. Res.*, *88*, 7647–7666.

McCave, I. N. (1984), Size spectra and aggregation of suspended particles in the deep ocean, *Deep Sea Res., Part A*, *31*(4), 329–352.

McCave, I. N. (1986), Local and global aspects of the bottom nepheloid layers in the world ocean, *Neth. J. Sea Res.*, *20*(2), 167–181.

McCave, I. N., and T. F. Gross (1991), In-situ measurements of particle settling velocity in the deep sea, *Mar. Geol.*, *99*(3–4), 403–411.

McCave, I. N., and L. Carter (1997), Recent sedimentation beneath the Deep Western Boundary Current off northern New Zealand, *Deep Sea Res., Part I*, *44*, 1203–1237.

McWilliams, J. C. (1985), Submesoscale, coherent vortices in the ocean, *Rev. Geophys.*, *23*, 165.

MERMEX group (2011), Marine ecosystems' responses to climatic and anthropogenic forcings in the Mediterranean, *Prog. Oceanogr.*, *91*, 97–166.

Mertens, C., and F. Schott (1998), Interannual variability of deep-water formation in the Northwestern Mediterranean, *J. Phys. Oceanogr.*, *28*(7), 1410–1424.

Moutin, T., F. Van Wambeke, and L. Prieur (2012), Introduction to the biogeochemistry from the oligotrophic to the ultra-oligotrophic Mediterranean (BOUM) experiment, *Biogeosciences*, *9*, 3817–3825.

Nortek (2001), Sediment concentration with acoustic backscattering instruments, *Nortek Tech. Notes N4000-712*, 5 pp. [Available at http://www.nortek-as.com/lib/technical-notes/sediments.]

Nyffeler, F., and C. H. Godet (1986), The structural parameters of the benthic nepheloid layer in the northeast Atlantic, *Deep Sea Res., Part A*, *33*(2), 195–207.

Ogston, A. S., T. M. Drexler, and P. Puig (2008), Sediment delivery, resuspension, and transport in two contrasting canyon environments in the southwest Gulf of Lions, *Cont. Shelf Res.*, *28*, 2000–2013.

Palanques, A., P. Puig, M. Latasa, and R. Scharek (2009), Deep sediment transport induced by storms and dense shelf-water cascading in the Northwestern Mediterranean basin, *Deep Sea Res., Part I*, *56*, 425–434.

Palanques, A., P. Puig, X. Durrieu de Madron, A. Sánchez-Vidal, C. Pascual, J. Martín, A. Calafat, S. Heussner, and M. Canals (2012), Sediment transport to the deep canyons and open-slope of the western Gulf of Lions during the 2006 intense cascading and open-sea convection period, *Prog. Oceanogr.*, *106*, 1–15.

Picheral, M., L. Guidi, L. Stemmann, D. M. Karl, G. Iddaoud, and G. Gorsky (2010), The Underwater Vision Profiler 5: An advanced instrument for high spatial resolution studies of particle size spectra and zooplankton, *Limnol. Oceanogr. Methods*, *8*, 462–473.

Puig, P., A. Palanques, D. L. Orange, G. Lastras, and M. Canals (2008), Dense shelf water cascades and sedimentary furrow formation in the Cap de Creus Canyon, northwestern Mediterranean Sea, *Cont. Shelf Res.*, *28*, 2017–2030.

Puig, P., et al. (2013), Thick bottom nepheloid layers in the western Mediterranean generated by deep dense shelf water cascading, *Prog. Oceanogr.*, *111*, 1–23.

Schroeder, K., A. Ribotti, M. Borghini, R. Sorgente, A. Perilli, and G. P. Gasparini (2008), An extensive western Mediterranean deep water renewal between 2004 and 2006, *Geophys. Res. Lett.*, *35*, L18605, doi:10.1029/2008GL035146.

Severin, T., P. Conan, X. Durrieu de Madron, L. Houpert, M. J. Oliver, L. Oriol, J. Caparros, J. Ghiglione, and M. Pujo-Pay (2014), Impact of open-ocean convection on nutrients, phytoplankton biomass and activity, *Deep Sea Res., Part I*, *94*, 62–71.

Séverin, T., et al. (2017), Open-ocean convection process: A driver of the winter nutrient supply and the spring phytoplankton distribution in the Northwestern Mediterranean Sea, *J. Geophys. Res. Oceans*, in press.

Stabholz M., X. Durrieu de Madron, A. Khripounoff, M. Canals, I. Taupier-Letage, P. Testor, S. Heussner, P. Kerhervé, L. Houpert, and N. Delsaut (2013), Impact of open-sea convection on particulate fluxes and sediment dynamics in the deep basin of the Gulf of Lions, *Biogeosciences*, *10*, 1097–1116.

Stemmann, L., L. Prieur, L. Legendre, I. Taupier-Letage, M. Picheral, L. Guidi, and G. Gorsky (2008), Effects of frontal processes on marine aggregate dynamics and fluxes: An interannual study in a permanent geostrophic front (NW Mediterranean), *J. Mar. Syst.*, *70*(1–2), 1–20.

Tamburini, C., et al. (2013), Deep-sea bioluminescence blooms after dense water formation at the ocean surface, *PLoS One*, *8*(7), e67523, doi:10.1371/journal.pone.0067523.

Testor, P. (2013), *DEWEX-MERMEX 2013 LEG1*, RV Le Suroît, doi:10.17600/13020010. [Available at http://campagnes.flotteoceanographique.fr/campagnes/13020010/fr/.]

Testor, P., and L. Coppola (2010), *MOOSE-GE*, doi:10.18142/235. [Available at http://campagnes.flotteoceanographique.fr/series/235/fr/.]

Testor, P., and J.-C. Gascard (2003), Large-scale spreading of deep waters in the western Mediterranean Sea by submesoscale coherent eddies, *J. Phys. Oceanogr.*, *33*, 75–87, doi:10.1175/1520-0485(2003)033<0075:LSSODW>2.0.CO;2.

Testor, P., and J.-C. Gascard (2006), Post-convection spreading phase in the Northwestern Mediterranean Sea, *Deep Sea Res., Part I*, *53*(5), 869–893, doi:10.1016/j.dsr.2006.02.004.

Thomsen, L, and G. Gust (2000), Sediment erosion thresholds and characteristics of resuspended aggregates on the western European continental margin, *Deep Sea Res., Part I*, *47*, 1881–1897.

Vangriesheim, A., and A. Khripounoff (1990), Near-bottom particle concentration and flux: Temporal variations observed with sediment traps and nepholometer on the Meriadzek Terrace, Bay of Biscay, *Prog. Oceanogr.*, *24*(1–4), 103–116.

White, A. E., R. M. Letelier, A. L. Whitmire, B. Barone, R. R. Bidigare, M. J. Church, and D. M. Karl (2015), Phenology of particle size distributions and primary productivity in the North Pacific subtropical gyre (Station ALOHA), *J. Geophys. Res. Oceans*, *120*, 7381–7399, doi:10.1002/2015JC010897.

Zúñiga, D., J. García-Orellana, A. Calafat, N. B. Price, T. Adatte, A. Sanchez-Vidal, M. Canals, J. A. Sanchez-Cabeza, P. Masqué, and J. Fabres (2007), Late Holocene fine-grained sediments of the Balearic Abyssal Plain, Western Mediterranean Sea, *Mar. Geol.*, *237*, 25–36.